

INVESTIGATION OF THE THERAPEUTIC EFFECT OF SODIUM BUTYRATE
IN CACO-2 COLON CANCER CELL LINE
BY USING ATR-FTIR SPECTROSCOPY

A THESIS SUBMITTED TO
THE GRADUATE SCHOOL OF NATURAL AND APPLIED SCIENCES
OF
MIDDLE EAST TECHNICAL UNIVERSITY

BY
BUKET ÇELİK

IN PARTIAL FULFILLMENT OF THE REQUIREMENTS
FOR
THE DEGREE OF MASTER OF SCIENCE
IN
MICRO NANO TECHNOLOGY

JANUARY 2018

Approval of the thesis:

**INVESTIGATION OF THE THERAPEUTIC EFFECT OF SODIUM
BUTYRATE IN CACO-2 COLON CANCER CELL LINE
BY USING ATR-FTIR SPECTROSCOPY**

submitted by **BUKET ÇELİK** in partial fulfillment of the requirements for the degree of **Master of Science** in **Micro Nanotechnology Department, Middle East Technical University** by,

Prof. Dr. Gülbin Dural Ünver
Dean, Graduate School of **Natural and Applied Sciences** -----

Assoc. Prof. Dr. Burcu Akata Kurç
Head of Department, **Micro and Nanotechnology** -----

Assoc. Prof. Dr. Alpan Bek
Supervisor, **Physics Dept., METU** -----

Dr. Nihal Şimşek Özek
Co-supervisor, **Biological Sciences Dept., Atatürk University** -----

Examining Committee Members:

Prof. Dr. Feride Severcan
Biological Sciences Dept., METU -----

Assoc. Prof. Dr. Alpan Bek
Physics Dept., METU -----

Assoc. Prof. Dr. Filiz Korkmaz Özkan
Dept. Of Electrical and Electronical Engineering., Atılım Uni. -----

Assoc. Prof. Dr Çağdaş Devrim Son
Biological Sciences Dept., METU -----

Prof. Dr. Hakan Altan
Physics Dept., METU -----

I hereby declare that all information in this document has been obtained and presented in accordance with academic rules and ethical conduct. I also declare that, as required by these rules and conduct, I have fully cited and referenced all material and results that are not original to this work.

Name, Last name: Buket Çelik

Signature:

ABSTRACT

INVESTIGATION OF THE THERAPEUTIC EFFECT OF SODIUM BUTYRATE IN CACO-2 COLON CANCER CELL LINE BY USING ATR-FTIR SPECTROSCOPY

Çelik Buket

M.Sc. in Micro Nano Technology

Supervisor: Assoc. Prof. Dr. Alpan Bek

Co-supervisor: Dr.Nihal Şimşek Özek

January 2018, 59 pages

Sodium butyrate (NaBt), as one of the HDACi, has been demonstrated that it induces apoptosis, cell cycle arrest, the inhibition of angiogenesis, metastasis and gene expression changes. To date, there are several studies performed to investigate its therapeutic effect; however, the exact mechanism at molecular level is not clear yet. Therefore, the current thesis was aimed to clarify the action/therapeutic potential mechanisms of sodium butyrate in Caco2 colon cancer cell line at molecular level using ATR-FTIR spectroscopy, quantitative spectral and chemometric analyses. 3mM, 6mM and 9mM doses of sodium butyrate were applied to Caco2 cell line for 12h, 24h and 48 h. According to the results, NaBt treatment caused an increase in the unsaturated lipids, implying elevated lipid peroxidation. Moreover increased saturated lipids, membrane fluidity/dynamics and esters and triacylglycerols were obtained in NaBt-treated groups with respect to the control ones. However, NaBt induced a degradation of proteins and nucleic acids. HCA and PCA results indicated that in all studied doses, there was a clear distinction between studied groups in a time dependent manner. The results of the current study implied that sodium

butyrate may have therapeutic potential by structural and functional remodelling of cancer cells.

Keywords: Caco2, colon cancer, molecular level, ATR-FTIR, PCA, HCA



ÖZ

SODYUM BÜTERATIN CACO2 KOLON KANSERİ HÜCRELERİ ÜZERİNDE TERAPATİK ETKİSİNİN ATR-FTIR SPEKTROSKOPİSİ KULLANILARAK İNCELENMESİ

Çelik Buket

M.Sc. in Mikro Nano Teknoloji

Tez Yöneticisi: Doç. Dr. Alpan Bek

Ortak Tez Yöneticisi: Dr.Nihal Şimşek Özek

Ocak 2018, 59 sayfa

Sodyum Büterat, HDACi'lerin bir çeşidi olup çoğalma, diferansiyasyon, hücre siklusu arresti, anjiyojenez engellemesi, metaztaz ve gen ekspresyonunu indüklemektedir. Şu zamana kadar, terapatik etkileri ile ilgili çeşitli çalışmalar var olup, moleküler düzeyde etki mekanizması bilinmemektedir. Bu tezin amacı aksiyon/terapatik potensiyel mekanizmasını Caco2 kanser hücreleri üzerinde ATR-FTIR spektroskopisi kullanarak spektral ve kemometrik analizler ile göstermektir. 3mM, 6mM ve 9 mM dozlarında sodyum büterat 12s, 24s ve 48s etki süreleri ile Caco2 hücrelerine uygulanmıştır. Aldığımız sonuçlara göre NaBt tedavisi doymamış yağların yoğunluğunda artışa sebep olup, bunun sebebi olarak da yağ peroksidasyonu gösterilmiştir. Buna ek olarak, doymuş yağlardaki, hücre zarı akışkanlığı/dinamiği, ester ve trigliseritte kontrol grubuna göre tedavi edilmiş grup artış göstermiştir. Bununla birlikte, NaBt Reaktif Oksijen Türleri (ROS) oluşumunu indüklemiş ve zamana bağlı olarak protein ve nükleik asitlerin azalmasına yol açmıştır. HCA ve PCA sonuçları tüm çalışılan gruplarda net bir ayrımın gözlemlendiğini belirlemiştir. Bu sonuçlar ile NaBt'ın kanser hücrelerinin yapısal ve fonksiyonel tekrar modellenmesi için kullanılabilceği söylenebilir.

Anahtar Kelimeler: Caco2, kolon kanseri, moleküler seviye, ATR-FTIR, PCA, HCA



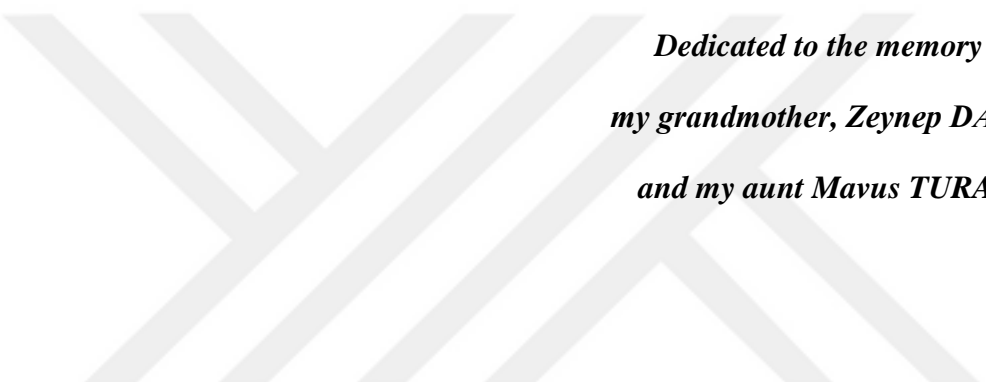
ACKNOWLEDGEMENTS

I would like to express my special thanks to my advisor Assoc. Prof. Dr. Alpan Bek for his patience motivation.

I am grateful to my co-advisor Dr. Nihal ŐimŐek zek for her valuable suggestions and guidance.

I would like to express my special thanks to Prof.Dr. Feride Severcan.

Finally, I must express my very profound gratitude to my mother Őule elik, to my father Bahaddin elik and my cat Elvis, for providing me with unfailing support and continuous encouragement throughout my years of study.



*Dedicated to the memory of
my grandmother, Zeynep DAĞ
and my aunt Mavus TURAN*

TABLE OF CONTENTS

ABSTRACT.....	v
ÖZ.....	vii
ACKNOWLEDGEMENTS	ix
TABLE OF CONTENTS	xi
LIST OF TABLES	xiii
LIST OF FIGURES	xiv
LIST OF ABBREVIATIONS	xvii
CHAPTERS	
1. INTRODUCTION.....	1
1.1. Histone deacetylases.....	1
1.1.1. Classes of HDACi.....	2
1.1.2 Histone deacetylase inhibitors in cancer research	5
1.1.3 The cellular effects of HDACi.....	5
1.1.4 Clinical development of HDACi	5
1.1.5 Sodium Butyrate as a HDAC inhibitor	6
1.1.6 Sodium Butyrate: a HDAC inhibitor in cancer research	6
1.1.7.HDACi s in Colorectal Cancer.....	7
1.3. Spectroscopy.....	8
1.3.1 Infrared Spectroscopy	10
1.3.1.1 Fourier Transform Infrared Technology.....	11
1.3.1.2 Attenuated Total Reflection Mode in FTIR Spectroscopy	14
1.3.1.3 Infrared Spectroscopy on Cancer Cells	17
1.4 Aim of the Study.....	21
2. MATERIAL AND METHODS	23
2.1 Cell Culture and Growing Conditions	23
2.2 Sodium Butyrate Treatments.....	23
2.3 ATR-FTIR Spectroscopic Study.....	24
2.4 Statistical Data Analysis	25
3. RESULTS AND DISCUSSION	27
3.1 Characterization of Sodium Butyrate Induced-Molecular Alterations in Colon Cancer Cells.....	27
3.1.1 ATR-FTIR Spectroscopy.....	27
4. CONCLUSION	49



LIST OF TABLES

Table 1 HDAC classification (Taken from Saharan et al. , 2011).....	3
Table 2 HDAC inhibitors (Taken from Bolden et al. 2006).....	4
Table 3 Band assignments of major absorptions in IR spectra of colon cancer cell in the 3030–900 cm ⁻¹ region based on literature (Choo et al., 1995, Jackson et al., 1998, Banyay et al., 2003, Ramesh et al., 2002, Mourant et al., 2003, Salman et al., 2001, Diem e	29



LIST OF FIGURES

Figure 1	HDAC inhibitor (Taken from Lane et al. , 2009).....	2
Figure 2	NaBt effect on human breast carcinoma cells (Taken from Soldatenkov et al. , 1998).....	8
Figure 3	Electromagnetic spectrum (Taken from https://nationalmaglab.org/images/about/around_the_lab/faraday_cage/faradaycage-emspectrum.gif).....	9
Figure 4	FTIR spectrum and corresponding changes (Taken from Baker et al. , 2014).....	10
Figure 5	Molecular vibrations (Taken from https://skechemistry.wikispaces.com/file/view/IR%20interactions.JPG/439462460/800x473/IR%20interactions.JPG).....	11
Figure 6	Michelson interferometer (Adapted from http://vlab.amrita.edu/?sub=1&brch=189&sim=1106&cnt=1).....	12
Figure 7	Single reflection ATR (Adapted from Pike Technologies,2011).....	15
Figure 8	Refraction (Adapted from http://www.ece.rice.edu/~gtm1/ELEC262/pdf/lecture14.pdf).....	16
Figure 9	Example of a dendrogram (Taken from Santos et al. , 2004).....	20
Figure 10	Clustering by PCA (Taken by Santos et al. ,2004).....	21
Figure 11	The representative spectra of control Caco2 cells in the 3030-900 cm^{-1} spectral region.	28
Figure 12	The representative spectra of control and 3mM NaBt treated Caco2 cells for 12h, 24h and 48h in the 3017-2800 cm^{-1} spectral region.	31
Figure 13	Band area of olefinic band (3008-3015 cm^{-1}) in control and 3mM NaBt treated (A), control and 6mM NaBt treated (B) control and 9mM NaBt (C) treated Caco2 cells for 12h,24h and 48h.	32
Figure 14	Band area of CH_2 antisymmetric stretching bands (2921-2851 cm^{-1}) in control and 3mM NaBt treated (A), control and 6mM NaBt treated (B) control and 9mM NaBt (C) treated Caco2 cells at 12h,24h and 48h.	33

Figure 15 Band width of CH ₂ antisymmetric stretching band (2921cm ⁻¹) in control and 3mM NaBt treated (A), control and 6mM NaBt treated (B) control and 9mM NaBt treated (C) Caco2 cells at 12h,24h and 48h.....	35
Figure 16 Wavenumber of CH ₂ antisymmetric stretching band (2921cm ⁻¹) in control and 3mM NaBt treated(A), control and 6mM NaBt treated (B) control and 9mM NaBt treated(C) Caco2 cells at 12h,24h and 48h.....	35
Figure 17 Band area of Ester C=O stretching band (1740cm ⁻¹) for control and 3mM NaBt (A), control and 6mM NaBt (B) control and 9mM NaBt (C) treated Caco2 cells at 12h,24h and 48h.....	36
Figure 18 The representative spectra of control and 3mM NaBt treated Caco2 cells for 12h, 24h and 48h in the 1800-900 cm ⁻¹ spectral region.....	37
Figure 19 Band area of Amide I band (1651cm ⁻¹) in control and 3mM NaBt treated(A), control and 6mM NaBt treated (B) control and 9mM NaBt treated (C) Caco2 cells at 12h, 24h and 48h	38
Figure 20 Band area of PO ₂ ⁻ antisymmetric and symmetric bands (1238 cm ⁻¹) in control and 3mM NaBt treated (A), control and 6mM NaBt treated (B) control and 9mM NaBt treated (C) Caco2 cells at 12h, 24h and 48h	39
Figure 21 Band area of Ribose Ring:RNA bands (1084 cm ⁻¹) in control and 3mM NaBt treated(A), control and 6mM NaBt treated(B) control and 9mM NaBt treated(C) Caco2 cells at 12h, 24h and 48h	40
Figure 22 PCA score plots of control, 3mM NaBt treated Caco2 cells at 12h,24h and 48h. PCA was performed with second derivative vector normalized spectra within the 4000-650cm ⁻¹ spectral range.....	42
Figure 23 PCA score plots of control, 6mM NaBt treated Caco2 cells at 12h,24h and 48h. PCA was performed with second derivative vector normalized spectra within the 4000-650cm ⁻¹ spectral range.....	42
Figure 24 PCA score plots of control, 9mM NaBt treated Caco2 cells at 12h,24h and 48h. PCA was performed with second derivative vector normalized spectra within the 4000-650cm ⁻¹ spectral range.....	43
Figure 25 PCA loading plot for 3mM in 4000-650 cm ⁻¹	43
Figure 26 PCA loading plot for 6mM in 4000-650 cm ⁻¹	44
Figure 27 PCA loading plot for 9mM in 4000-650 cm ⁻¹	44

Figure 28 Hierarchical clustering of the 3mM NaBt treated Caco2 cell lines within different time durations as control, 12h,24h and 48h. Clustering was performed using Ward’s algorithm and second derivative vector normalized spectra within the 4000-650cm⁻¹ spectral..... 45

Figure 29 Hierarchical clustering of the 6mM NaBt treated Caco2 cell lines within different time durations as control, 12h,24h and 48h. Clustering was performed using Ward’s algorithm and second derivative vector normalized spectra within the 4000-650cm⁻¹ spectra 46

Figure 30 Hierarchical clustering of the 9mM NaBt treated Caco2 cell lines within different time durations as control, 12h,24h and 48h. Clustering was performed using Ward’s algorithm and second derivative vector normalized spectra within the 4000-650cm⁻¹ spectral 47

LIST OF ABBREVIATIONS

ATR	Attenuated Total Reflectance
FTIR	Fourier Transform Infrared
HAT	Histone Acetylase Transferase
HDAC	Histone Deacetylase
HDACi	Histone Deacetylase Inhibitor
NaBt	Sodium Butyrate
PCA	Principal Component Analysis
HCA	Hierarchical Cluster Analysis

CHAPTER I

INTRODUCTION

Colorectal cancer is one of the most common cancer types which accounts for over 9% of cancer cases. It has been the third most common cancer around the World and fourth main cause for death. It does not differentiate between man and women with the highest rates around the countries as Australia, New Zeland, US and Europe. South Africa, China and India are the countries that has the lowest colorectal cancer rates (Hagggar et al. , 2009). In Melbourne, Australia, a comprehensive study has showed that hypertension, stroke, chronic arhritis, heart disease, chronic chest disease and hemorrhoids are the most common symptoms for the colorectal cancer (Kune et al. , 1988). Recent studies proved that histone deacetylases inhibitors (HDACi) are considered as a powerful drug for colorectal cancer.

In this thesis, therapeutic effects of three different doses of sodium butyrate (3mM,6mM and 9mM) has been investigated with different time dependencies (12h, 24h and 48h) by using ATR-FTIR spectroscopy based on spectroscopic and unsupervised chemometric analysis.

1.1. Histondeacetylases

The DNA sequence is the provider for the genetic code of the proteins. Expression and suppression of the transcription process is determined by the chromatin structure which is also referred to epigenetic gene regulation. Acetylation/deacetylation of the core histones are one of the most researched areas for the epigenetic modifications. Normal cell growth has been highly associated with the balance between acetylation and deacetylation. Structural alterations cause abnormal cell growth that may lead to cancer. (Marks et al. , 2004)

Epigenetic modulations play a crucial regulatory role in cell biology. DNA is packaged into an organized structure, the nucleosome, in the context of gene

regulation. Nucleosome consists of a DNA strand wrapped around the core of eight histone proteins. Each histone has N-terminal tails which extends outward through the DNA strand. These histone tails have amino acid residues that can be modified by post-translational acetylation, methylation and phosphorylation. Through these processes, secondary structure of these histone tails are modified. Furthermore, this modification leads to an increase in the distance between histones and DNA. Due to this distance increment, the accessibility of transcription factors to gene promoter regions is increased. For decreasing the accessibility, deacetylation, demethylation and dephosphorylation can be occurred.

Both developmental and regulatory cell processes are significantly influenced by histone modification, which may lead to diseases like cancer. Histone acetyl transferases (HAT) is responsible for histone acetylation and histone deacetylases (HDAC) is the enzyme responsible for the removal of the acetyl groups. HDAC inhibitors are considered to have a significant potential for the cancer treatment. In the figure below (Figure 1), HDAC6 is attached to Heat Shock Protein 90 (HSP90) which enables it to bind to cancer protein X. With the usage of HDAC inhibitor, HDAC6 can be inhibited so cancer protein X can be released and degraded

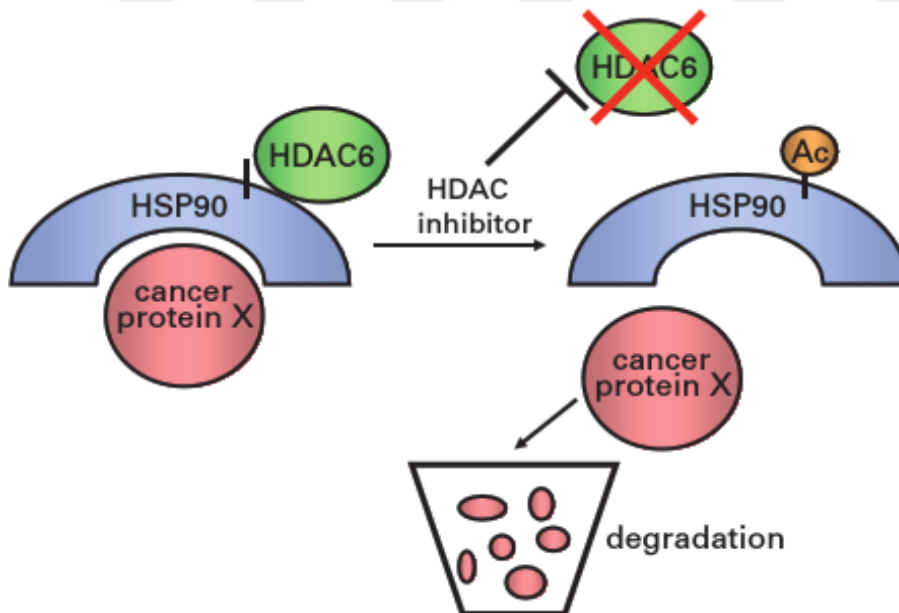


Figure 1 HDAC inhibitor (Taken from Lane et al. , 2009)

1.1.1. Classes of HDACi

In order to understand HDAC inhibitor classification, HDAC classification must be done first.

There are two types of HDAC enzymes: Zn dependent and NAD⁺ dependent which means that one group needs Zn as cofactor while the other group needs NAD⁺. Zn dependent HDACs can be divided into two classes as Class I and Class II. NAD⁺-dependent HDACs have only Class III (Table 1).

Table 1 HDAC classification (Taken from Saharan et al. , 2011)

Zn -Dependant HDAC		NAD- Dependant HDAC
Inhibited by TSA		Inhibited by Nicotinamide
Class I	Class II	Class III
HDAC 1	HDAC 4-7	SIRT 1-7
HDAC 2	HDAC 9	
HDAC 3	HDAC 10	
HDAC 8		
HDAC 11		

Class I HDACs are homologous to the yeast RPD3 protein and it is primarily detected in the cell nucleus. However, HDAC8 can be found in the cytoplasm or membrane. Target histones have relatively small aminoacids and carboxy terminal extensions. Due to these reasons, Class I selective enzymes play a significant role in cell survival, proliferation and differentiation.

Class II HDACs are homologous to the yeast Hda1 protein which are larger than Class I and typically plays role in both histone and non-histone proteins. Class II ones have more tissue specific regulatory function than Class I ones which are expressed in a limited cell type and either shutters between the nucleus and cytoplasm and in some situations, mainly stay in cytoplasm.

Class III is also called as sirtuins which are homologous of the yeast protein Sir2. The purpose of the Class III enzymes is to regulate gene expression as a response to cellular redox status changes (Dokmanovic et al. , 2007).

HDACi can be classified as hydroxamates, cyclic peptides, aliphatic acids and benzamides. Hydroxamate class can transform cell proliferation at nanomolar concentrations (

Table 2). The cyclic peptide class is a complex group that contains depsipeptide, apicidin and the cyclic hydroxamic acid-containing peptide group of molecules and it is also active in nanomolar concentrations like hydroxamates. The aliphatic acid class consists of relatively weaker inhibitors and they become active in milimolar concentrations (Marks et al. , 2004).

Table 2 HDAC inhibitors (Taken from Bolden et al. 2006)

Class	Compound	[range]	HDAC specificity	Clinical trials
Short-chain fatty acid	Butyrate	mM	Class I, IIa ¹²¹	Phase I, II
	Valproic acid (VPA)	mM	Class I, IIa ¹²¹	Phase I, II
	AN-9 (prodrug)	μM	N/A	Phase I, II
Hydroxamate	Trichostatin A (TSA)	nM	Class I, II ¹²¹	N/A
	Suberoylanilide hydroxamic acid (SAHA, Vorinostat)	μM	Class I, II ¹²¹	Phase I, II, III (pre -registration)
	PXD101	μM	Class I, II ¹²¹	Phase I
	Oxamflatin	μM	N/A	N/A
	LAQ824	nM	Class I, II ¹²¹	Phase I
	LBH589	nM	Class I, II ¹²¹	Phase I
	<i>m</i> -carboxycinnamic acid bis-hydroxamide (CBHA)	μM	N/A	N/A
	Scriptaid	μM	N/A	N/A
	Pyroxamide	μM	Class I, unknown effect on class II ¹⁷⁶	Phase I
	Suberic bishydroxamic acid (SBHA)	μM	N/A	N/A
	Azelaic bishydroxamic acid (ABHA)	μM	N/A	N/A
	SK-7041	nM	HDACs 1 and 2 ¹⁷⁷	N/A
	SK-7068	nM	HDACs 1 and 2 ¹⁷⁷	N/A
	CG-1521	μM	N/A	N/A
	Tubacin	μM	Class IIb ³⁹	N/A
Benzamide	MS-275	μM	HDACs 1, 2,3, 8 (marginally) ¹⁴	Phase I, II
	CI-994 (tacedinaline)	μM	N/A	Phase I, II, III
Cyclic tetrapeptide	Depsipeptide	nM	Class I ⁸⁶	Phase I, II
	Trapoxin A	nM	Class I, IIa ¹²¹	N/A
	Apicidin	nM	HDACs 1 and 3, not HDAC8 ¹⁷⁰	N/A
	CHAPs	nM	Class I ¹⁷⁸	N/A
Electrophilic ketone	Trifluoromethylketone	μM	N/A	N/A
Miscellaneous	Depudecin	μM	Class I, unknown effect on class II ¹⁷⁹	N/A
	MGCD-0103		Class I ²⁰⁵	Phase I

1.1.2 Histone deacetylase inhibitors in cancer research

Histone deacetylases have been investigated over the last decade for mainly two reasons. One of them is, they have been associated with the pathogenesis side of the cancer. The second reason is that their ability to interfere with HDAC activity and lead to significant biological changes. This ability has been tested and verified by clinical trials with encouraging results with time and dose dependent manners (Minucci et al. 2006).

1.1.3 The cellular effects of HDACi

The cellular effects of HDAC mostly related their inhibitor effects of histone acetyl transferases (HATs) activity which plays a significant role in gene expression. Therefore, mutations occurred in HDAC codes may cause tumor development. The reason behind this hypothesis is that HDAC codes regulate significant cellular functions like cell proliferation, apoptosis and differentiation. Replication of the genetic material and cell division results in two daughter cells, is the simple definition of cell proliferation of mammals. On the other hand, termination of cell differentiation is the loss of cell proliferation potential. Regulation of cell proliferation and differentiation is both done by growth stimulatory and growth inhibitory factors. (Antonio, 1988) For this reason, HDACi are investigated for regulating these processors and stopping tumor development (Ropero et al.,2007). Therefore, they are strongly suggested as a chemotherapeutic agent or adjuvant.

1.1.4 Clinical development of HDACi

The FDA, for now, has approved three of the HDAC inhibitors for T-cell lymphoma while many of the HDAC inhibitors are still in clinical development stages. The first drug approved is the “Varinostat-SAHA” and Zolima developed by Merck Co. Inc. and approved in 2006. This drug is used for T-Cell Lymphoma and non-Hodgkin’s lymphoma. Structure of the Varinostat is the hydroxamic acid and it is originally used as antifungal. The second drug is approved in 2009 and it is the “Romidepsin” which is developed by Gloucester Pharmaceuticals. This drug is also used for T-cell lymphoma. Romidepsin is produced with the isolation from Chromobacterium Violaceum cultures. The third drug is the “Belinostat” which is developed by

Spectrum Pharmaceuticals and it is approved in 2014. It is used for refractory T-cell lymphoma. (Rashidi et al. , 2015).

1.1.5 Sodium Butyrate as a HDAC inhibitor

Butyrate is normally produced in healthy human colon by anaerobic bacterial fermentation and it is a short-chain fatty acid. The rate of butyrate formation is mostly influenced by diet. It has been well known that a range of biological processes are strongly influenced by butyrate .Moreover, the butyrate and its analogues can be used to treat human diseases like cancer and bowel inflammatory diseases. From many studies, butyrate is claimed to inhibit colon cancer development (Kaboyashi, 1998).

1.1.6 Sodium Butyrate: a HDAC inhibitor in cancer research

In 1970s, Sodium Butyrate (NaBt) is reported as halting DNA synthesis, initiates cell proliferation, differentiate cell morphology and cause an increase or a decrease in gene expression. Ingram and his colleagues discovered that sodium butyrate caused an increased acetylated histones in HeLa and Friend erythroleukemic cells (Davie, 2003). There is still little information about the metabolism of butyrate in cultured colon cancer cells. The reason for this is that butyrate arrests the growth of colon cancer cells rapidly to some extent. Studies with limited data showed that differentiated Caco2 cells used butyrate faster than nondifferentiated Caco2 cells. In one of the studies, Caco2 cells treated with NaBt for 72h at various stages of differentiation. The results showed that NaBt induced apoptosis in predifferentiated Caco2 cells and not in differentiated ones. According to these results, it is stated that NaBt may play a crucial role in inducing apoptosis. In some studies, butyrate reduced tumorigenesis in vivo which can be stated as evidence that NaBt can reduce the colon cancer risk. For humans, there is an indirect proof for the protective role of butyrate on colon cancer which is a lowering effect of butyrate on polyps as compared to the control group (Kobayashi, 1998). Moreover, various antiproliferative effects of NaBt have been demonstrated in colon cancer cell cultures. The effects of butyrate on cell cycle progression including growth arrest in G1 phase and the induction of terminal differentiation have been also indicated. In addition to these, among the

differentiated mammalian cells that are in cell culture, NaBt has been reported to alter the cell membrane composition, enzyme activity changes and gene expression modulations (Toscani, 1988).

1.1.7.HDACi s in Colorectal Cancer

In Wiechert et al. study, the lack of translational information by HDAC-Class 1 isoform expression functions and patterns with colorectal tumors are studied. The aim of this study was to specify HDAC isoforms that are significant for tumorigenesis of colorectal cancer. The results showed that class-1 HDACs especially HDAC2 (HDAC-1, P =0.008; HDAC-2, P = 0.017; HDAC-3, P = 0.005) played a significant role for survival rates in colorectal cancer (Weichert et al. , 2008). From this study, we can conclude that HDACi should be chosen accordingly for the class of HDACs.

1.2.2.1 Sodium Butyrate as a HDAC inhibitor and Colorectal Cancer

The mechanism underlying the influences of NaBt on the cell functions has not been elucidated yet; however, it is considered that its effect is on the regulation of gene expression and it is mostly deacetylation of histones. NaBt have other effects besides deacetylation of histones, such as the alteration of DNA methylation, the intracellular kinase signalling modulation and the inhibition of histone phosphorylation. However, studies showed that cancer cells are more sensitive to HDAC inhibition. The effect of NaBt on the plasminogen/plasmin system has been demonstrated (Brumer et al. , 1981). Correlation between the increase in tumour and serum levels of PPS and invasive tumour cell phenotype has been found. Both in vivo and in vitro studies showed that NaBt decreased the plasminogen activator activity by balancing the components of the PPS. Other effects of NaBt in multiple colonic cancer cell lines are the enhancement of the detoxifying enzyme glutathion-S-transferase activity. In addition, NaBt also may inhibit the tumour cell migration due to the inhibition of the decy-accelarating factor expression. The last effect is due to the modulation of the vascular endothelial growth factor and hypoxia-inducible factor which are angiogenesis related protein and the modulation of these proteins, leading to the inhibition of tumour-induced angiogenesis (Brumer et al. , 1981).

In the Figure 2, the effects of sodium butyrate on the MCF-7 human breast carcinoma cells, which is the induction of the cell death, are shown. This is a time-dependent study in which cells are given 3mM sodium butyrate and cells are treated for 0 h in (a), 24 h in (b) and 48 h in (c) and (d). It can be seen that in (d), cell death has occurred for 3 mM 48 h treated case. Living cells (green), dying cells (yellow), and dead cells (red) and image are produced by two-colour fluorescence cell viability assay and it is photographed under a Zeiss fluorescence microscope with excitation at 495nm (Soldatenkov et al. , 1998).

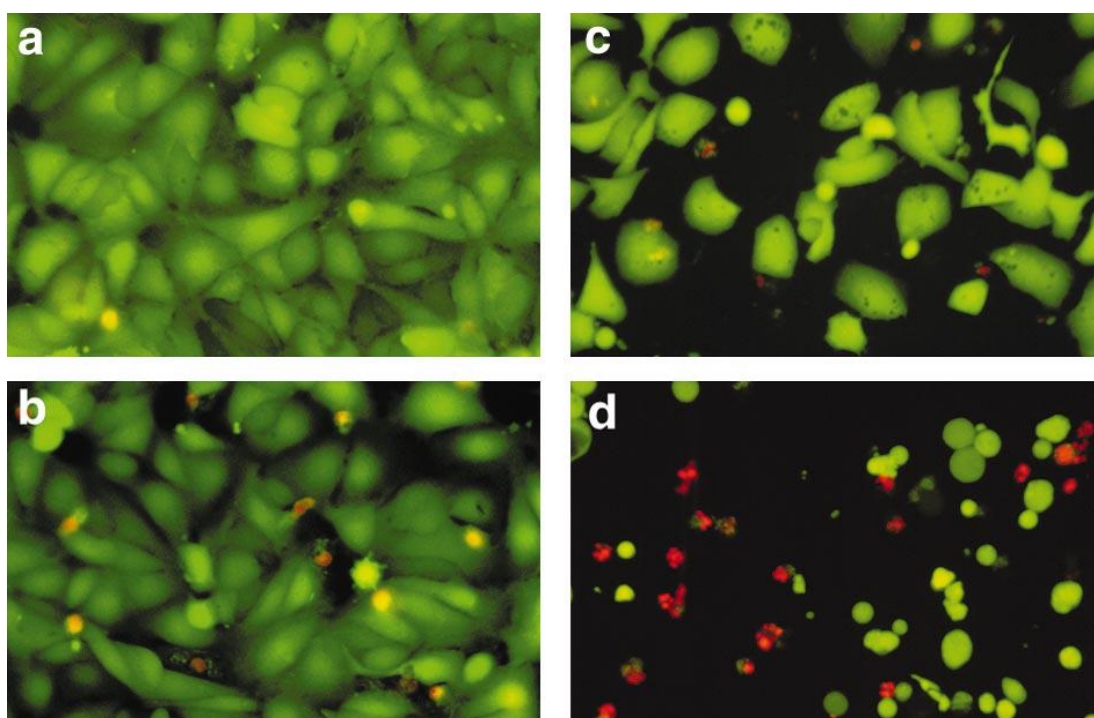


Figure 2 NaBt effect on human breast carcinoma cells (Taken from Soldatenkov et al. , 1998)

1.3. Spectroscopy

Spectroscopy studies the interaction between the EM light and the matter, dependent on the wavelength. The result of this interaction leads to different peaks at different wavelengths, which is called as spectrum. Spectrum is a function of wavelength and it is used to identify samples and its ingredients. Photons are grouped as UV, VIS, NIR, IR, terrahertz etc. within the electromagnetic spectrum (Figure 3).

Electromagnetic Spectrum

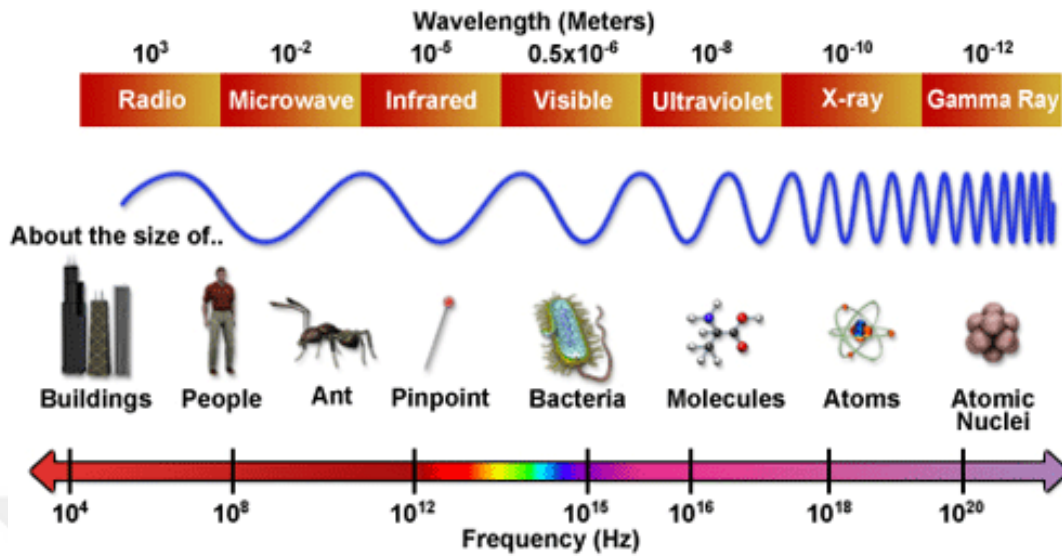


Figure 3 Electromagnetic spectrum (Taken from https://nationalmaglab.org/images/about/around_the_lab/faraday_cage/faradaycage-emspectrum.gif)

Transition between energy levels of the electrons are caused by the interaction between the EM wave and the matter.

The total energy of the molecule can be expressed as in [1]:

$$E_{molecular} = E_{electronic} + E_{vibrational} + E_{rotational} + E_{translational} \quad [1]$$

Electronic, rotational and vibrational spectroscopy is based on the quantization of the energies. The “molecule” refers to a stabilized system with nuclei and electrons. If the proton and electron numbers are unequal, the system is called as molecular ion.

Transition between electronic energy levels result in UV absorption, vibrational levels result in VIS/IR, rotational levels result in mm wave region. So, infrared spectroscopy studies the changes in vibrational levels.

1.3.1 Infrared Spectroscopy

Infrared spectroscopy is one of the most significant techniques that scientists use in the last decades. Samples in any state (liquid, powder etc.) can be studied non-destructively which provides an important advantage. Infrared spectrometers are on the market since 1940s. It first started with dispersive spectrometers that contains prisms or gratings. Application of Fourier Transform to spectroscopy is an important step to scan samples quickly with high scan rates (Stuart, 2004).

IR spectra gives information about molecular vibrations. The most commonly used infrared region is $400\text{-}4000\text{cm}^{-1}$. For biological materials, most significant regions are:

- Fingerprint region: $600\text{-}1450\text{ cm}^{-1}$
- Amide I and Amide II region: $1500\text{-}1700\text{cm}^{-1}$
- Stretching vibrations (e.g. S-H, C-H, N-H and O-H): $2550\text{-}3500\text{cm}^{-1}$ (Baker et al. , 2014) (Figure 4).

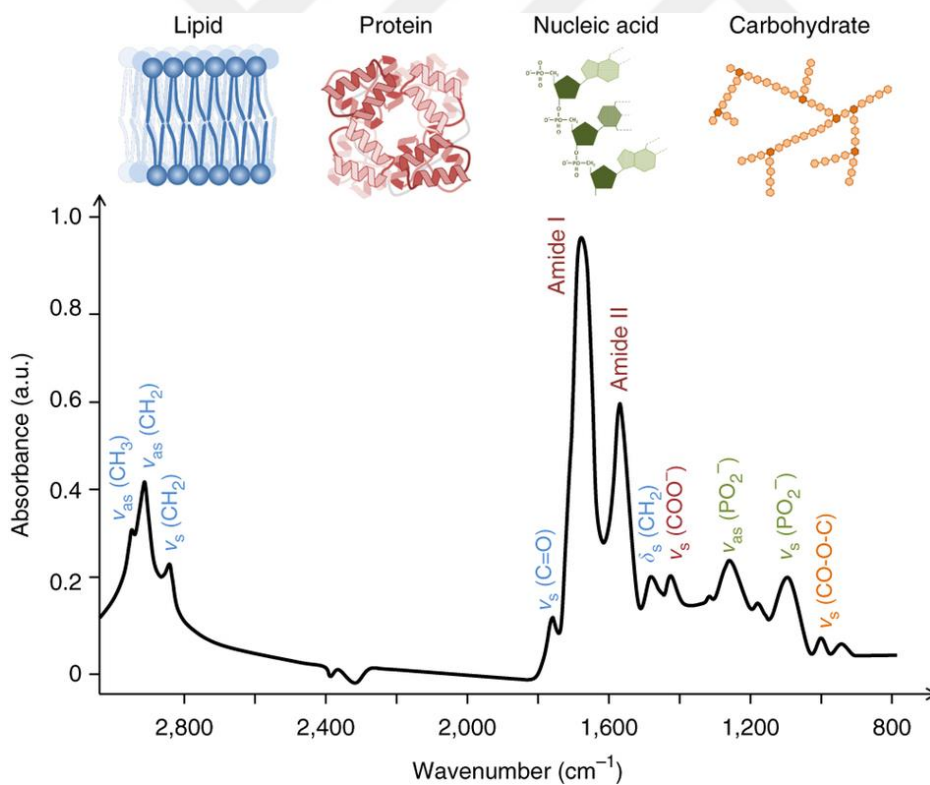


Figure 4 FTIR spectrum and corresponding changes (Taken from Baker et al. , 2014)

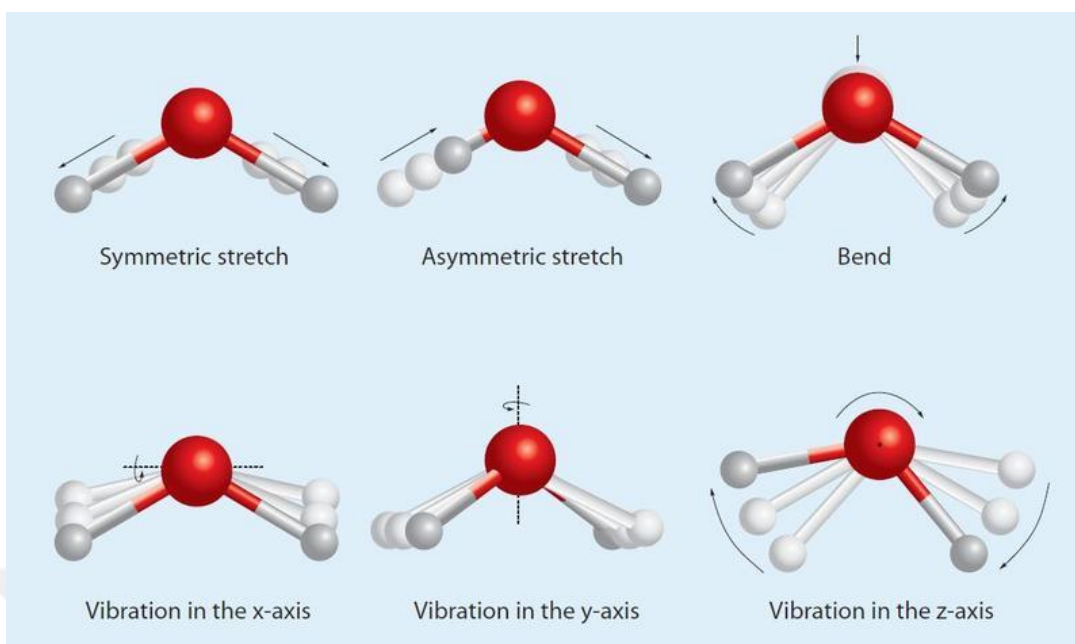


Figure 5 Molecular vibrations (Taken from <https://skcchemistry.wikispaces.com/file/view/IR%20interactions.JPG/439462460/800x473/IR%20interactions.JPG>)

A molecule consisting of N atoms have $3N$ degrees of freedom in the 3-dimensional space. There are 3 translational and 3 rotational vibrations (Figure 5) so a molecule have $3N-6$ degrees of freedom however, if it is linear, it will have $3N-5$ degrees of freedom.

1.3.1.1 Fourier Transform Infrared Technology

Before FT, spectrometers consisted of prisms and gratings that disperse light and then detects separately each wavelength. After that, spectrometers are used with Michelson interferometer, which all wavelengths enter to interferometer and detected together and than fourier transform is applied and given result is given in the frequency domain.

The Michelson interferometer (Figure 6) was invented by Albert Michelson in 1893 and it is the best example for amplitude-splitting interferometry.

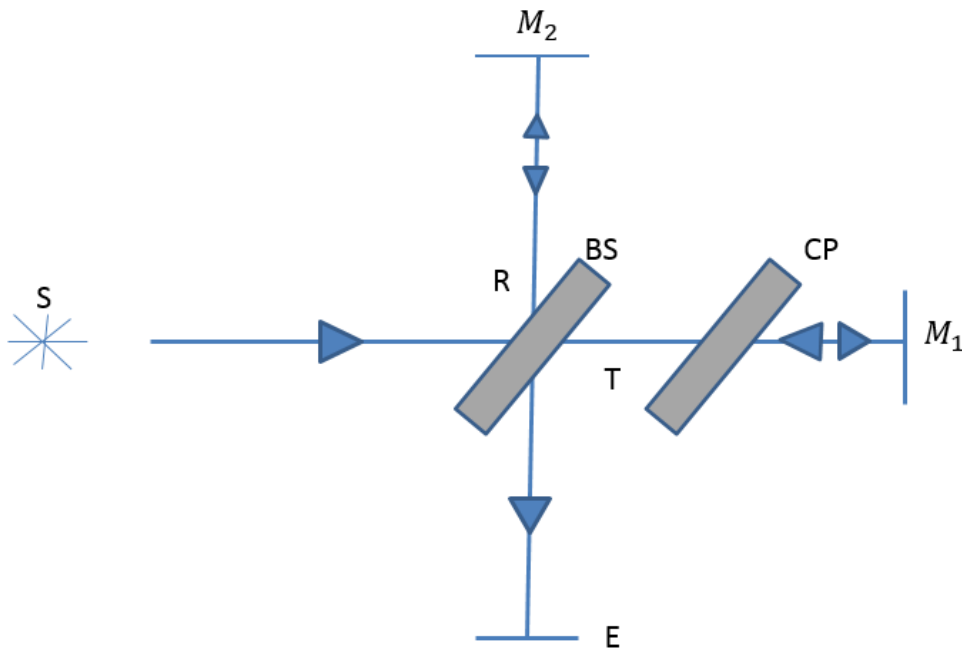


Figure 6 Michelson interferometer (Adapted from <http://vlab.amrita.edu/?sub=1&brch=189&sim=1106&cnt=1>)

S is a monochromatic source and beam splitter (BS), oriented at an angle 45° , divides the light coming from S into two beams with equal intensities. One part of the beam is transmitted (T) to mirror M_1 and reflected back to BS. After that, the beam splits again and 50% of the beam strikes the screen (E). The other part of the beam is reflected (R) to mirror M_2 which reflects it back to BS and then 50% of the beam reaches to the screen.

The reflective surface of the BS is on the lower right which causes the beam that is undergoing reflection at M_2 to pass through BS three times, whereas the beam reflected from M_1 passes through BS only once. Furthermore, the optical path length depends on the glass plate's index of refraction, which is the cause of optical path difference. To compensate for this phenomenon, a glass plate CP is placed that has the same thickness and index of refraction as the BS. The recombination of these two beams interferes and creates fringes on the screen E. The constructive and destructive interferences of these two beams are caused by the relative phase differences.

$$\text{Phase difference } \delta = \frac{2\pi x}{\lambda} = \frac{2\pi}{\lambda} 2nd \cos \theta \quad [1]$$

Intensity maxima is obtained by the following condition in [2].

$$\delta = l2\pi \quad l = 0, \pm 1, \pm 2, \pm 3 \dots \quad [2]$$

Merge [1] and [2] so we have [3];

$$l\lambda = 2nd\cos(\theta) \quad [3]$$

Assume the rays propagates in the direction of the optical axis $\theta=0$ and medium is vacuum $n=1$.

Then the equation [1] becomes $x=2d$.

Intensity of the interference of the two equal electromagnetic beams:

$$F = 2I_0[1 + \cos(2\pi v2d)] \quad [4]$$

If the optical path difference is given as x , the infinitesimal spectral element between $v+dv$:

$$dF(x, v) = 2E(v)[1 + \cos(2\pi vx)]dv \quad [5]$$

$$F(x) = 2 \int_0^{\infty} E(v)[1 + \cos(2\pi vx)]dv \quad [6]$$

Constant term is:

$$\frac{1}{2}F(0) = 2 \int_0^{\infty} E(v)dv \quad [7]$$

$I(x)$ can be found with subtracting [7] from [6] which is:

$$I(x) = 2 \int_0^{\infty} E(v) \cos(2\pi vx) dv \quad [8]$$

[8] is what we call as “interferogram”.

Since $E(v)=E(-v)$;

$$I(x) = \int_{-\infty}^{\infty} E(v) \cos(2\pi vx) dv = \int_{-\infty}^{\infty} E(v) e^{i2\pi vx} dv = F\{E(v)\} \quad [9]$$

$$I(x) = \int_{-\infty}^{\infty} E(v) e^{i2\pi vx} dv = F\{E(v)\} \quad [10]$$

$$E(\nu) = \int_{-\infty}^{\infty} I(x) e^{-i2\pi\nu x} dx = F^{-1}\{I(x)\} \quad [11]$$

Seen by the equations [10] and [11] with the change in optical path difference, one can switch to frequency space with taking inverse Fourier transform.

There are six main advantages of using interferometer beside the dispersive techniques:

- Firstly, measurements can be done simultaneously which is known as Fellgett Advantage. Rapid collection of the complete spectrum and multiple scans in shorter time durations are provided.
- The second advantage is the throughput advantage which is also known as Jacquinot advantage. For dispersive techniques, every throughput is bounded by the number of slits however, for interferometric techniques higher SNR is achieved with shorter time periods.
- The third advantage is known as Connes advantage which is the internal reference for each scan is provided by the HeNe laser. The wavelength of this laser is well known and calibration can be done much more accurately which provides long term stability rather than dispersive techniques.
- The fourth one is that interferometer modulates each wavelength of the source which provides lower stray light.
- The fifth advantage is the constant resolution which is defined by the Jacquinot stop aperture size and it does not change during the data collection. However, for the dispersive methods, optimization is made by adjusting the width of the slits during the scan, SNR stays constant while the resolution changes. But for the interferometer, SNR varies across the spectrum while the resolution is constant.
- The last advantage is that there are no discontinuities in the spectrum since there are no gratings (Antolasic, 2009).
-

1.3.1.2 Attenuated Total Reflection Mode in FTIR Spectroscopy

Attenuated total reflectance (ATR) is one of the most used FTIR sampling technique. ATR provides easy sample preparation for both qualitative and quantitative analysis.

A relatively higher refractive index crystal is used while IR beam directed onto the sample. Due to the change in refractive index, the IR beam reflects from the crystal's internal surface and creates an evanescent wave. Created evanescent wave projects into the sample while it is in intimate contact with the ATR crystal. One part of the energy of the evanescent wave is absorbed by the sample while some of them are reflected onto the crystal(Pike Technologies, 2011) (Figure 7).

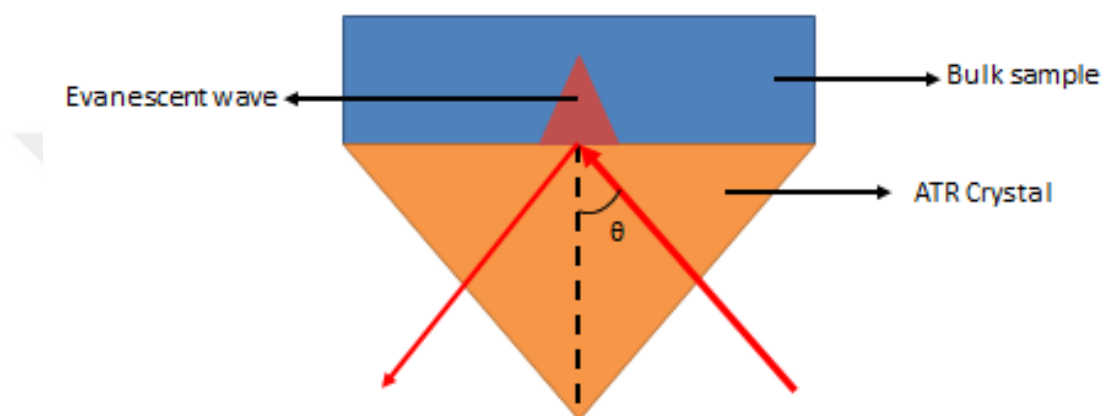


Figure 7 Single refraction ATR (Adapted from Pike Technologies,2011)

ATR can measure the changes that happen when internally reflected IR beam contacts with the sample. The main idea to have a higher refractive index crystal is to create evanescent waves that extends beyond the surface. The created evanescent waves protrude only few microns into the sample. This means that sample should be in direct contact with the crystal, otherwise waves may not reach into the sample.

Accordingly with the sample's nature, some part of the energy in the infrared spectrum is absorbed so the evanescent wave can be attenuated. This attenuated wave then exits from the other end of the crystal and detected by the IR detector. With the signal that detector get, an infrared spectrum is created (Perkin Elmer Technical Note, 2005).

So what is an evanescent wave and how is it created? It is all about the phenomenon of total internal reflection.

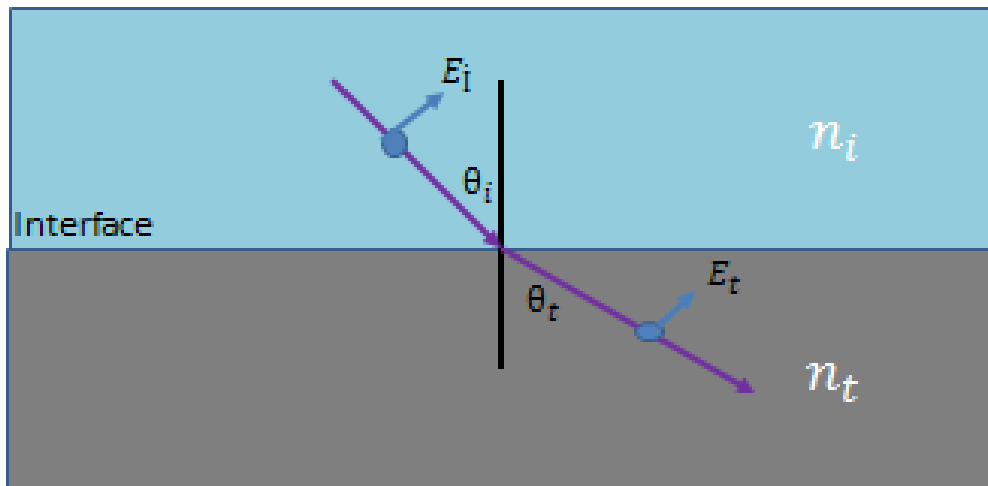


Figure 8 Refraction (Adapted from <http://www.ece.rice.edu/~gtn1/ELEC262/pdf/lecture14.pdf>)

Snell's law:

$$n_i \sin \theta_i = n_t \sin \theta_t \quad [1]$$

$$\theta_t = \sin^{-1} \left(\frac{n_i}{n_t} \sin \theta_i \right) \quad [2]$$

n_i : incidence side refractive index

n_t : transmission side refractive index

θ_i : Incident angle

θ_t : Transmission angle

Total internal reflection (TIR) occurs for the case $\theta_t = \frac{\pi}{2}$;

Using the Equation [3], it is clear that $\sin \theta_i > 1$ which makes $\cos \theta_i$ an imaginary number.

By using Euler formula, wave can be described as Equation [4]:

$$E' = E_0 e^{i(\vec{k} \cdot \vec{x} - \omega t)} \quad [4]$$

2D interpretation of Equation [4] is Equation [5]:

$$E' = E_0 e^{i(\vec{k}_x \cdot \vec{x} + \vec{k}_y \cdot \vec{y} - \omega t)} \quad [5]$$

E: Electric field

k: Wavenumber

x,y: Position

w: Angular frequency

t: Time

c: Speed of light

k can be stated as Equation [7]:

$$|\vec{k}| = \frac{n_t \omega}{c} \quad [6]$$

Through inserting Equation [7] into Equation [6] and solve it for the imaginary $\cos \theta_i = i\xi$:

$$Re\{\vec{E}\} = \vec{E}_0 \cos\left(\frac{n_t \omega}{c} \sin \theta_i y - \omega t\right) e^{-\frac{n_t \omega}{c} \xi x} \quad [7]$$

Cosinus part of the Equation [7] states that it is planar wave propagating in y direction, while exponential part states an exponential decay in the x direction. This is a localized wave which does not propagate in space and it is also known as evanescent waves.

1.3.1.3 Infrared Spectroscopy on Cancer Cells

The promising areas that FTIR spectroscopy can be used for cancer research are (Sahu et al. , 2005):

- To differentiate healthy and cancerous cells, tissues in organs such as breast, liver, colon etc., Lewis et al. states that in fingerprint region FTIR wavenumbers can interpret the glycogen levels that discriminates the adenocarcinoma tumours from normal tissue (Lewis et al. , 2010).
- To monitor in tissue level, abnormal cell growth and proliferation. Mourant et al. investigated the changes in the mammalian cells to find out whether they are in the exponential or plateau phase of growth by using FTIR . They have found out that the average absorbance per cell is lower in the pleateu phase than exponential phase of growth that can be measured by FTIR spectroscopy. (Maurant et al. , 2003)

- To distinguish abnormalities in cell-cell scrapings from small organs like thyroid etc., Cohenford et al. has evaluated the cervical samples of 22 women and 10 of them has no history of cervical cancer. Their data showed that mid-IR spectra between malignant and normal cervical samples differ significantly (Cohenford et al. 1998).
- To monitor the effect of chemotherapeutic effects of agents/drugs on tumor growth. Singh et al. have conducted two sets of experiments, in the first set, they have shown that the FTIR provides a fast sampling for investigating the modification due to propionylation. In the second set, they have demonstrated that with FTIR, APAP induced hepatotoxicity can be detected and diagnosed (Singh et al. , 2012).

In addition, IR spectroscopy is a useful tool to study biofluids like saliva, serum, urine or blood to obtain results rapidly and non-invasively while the samples are easily prepared (Baker et al. , 2014)

Here are several studies that used infrared spectroscopy for the cancer research:

In 1990, Rigas et al. proved that there is a difference between the FTIR spectra between normal and cancerous tissues that are resected from 11 colon cancer patients. They proposed that there is a change in band intensities at certain wavelengths, especially the wavelengths that correspond to phosphates and nucleic acid bands (Rigas et al., 1990).

In 2002, Argov et al. demonstrated a comparison that directly shows the difference between normal and cancerous samples/tissues that are removed from polypoid lesions in three patients. They claimed that the FT-IR signal demonstrates the biochemistry change that occurs in early neoplastic change in adenomas. 24 patients were included in the study which generates 300 spectra to analyze. Artificial neuronal network analysis was used for spectral analysis to create a prediction model and differentiate the morphological differences. From the peak analysis that are performed on only 3 patients, RNA/DNA ratio was observed results showed that it increase with the malignancy (Argov et al., 2002).

In 2005, Li et al. showed the results for their in vivo study on colon. Although a small number of samples were included, with the use of fibre-optic ATR FTIR

spectroscopy, results showed that there is change in bands especially of carbonyl, methylene and methyl (Li et al.,2005).

In 2009, Kendall et al. took a section of cancerous tissue and produced a variety of false color maps to compare these images with different computer techniques. They produced detailed spatial information for comparison (Kendall et al., 2009).

In 2015, Griggs et al. , identified biomolecular information from the maps, to make the comparison between normal, cancerous or inflamed in the tissues (Griggs et al., 2015).

1.3.1.2 Multivariate Analysis in Biospectroscopy

There are two unsupervised methods for pattern recognition which are Hierarchical Cluster Analysis (HCA) and Principal Component Analysis (PCA).

Biological system's FTIR spectra is quite complex due to the overlapping absorption of biomolecules. This is the challenge for extracting non-redundant and important information from the spectra. So, it is necessary to apply multivariate analysis to process this high-dimensional data (Ami et al. , 2012).

Quantitative Analysis

Hierarchical Cluster Analysis

HCA groups the samples in a plot called dendrogram by calculating the distance between them. Distance calculation can be done by utilizing different methods like Manhattan, Euclidean or Mahalanobis distance using the equation [1] for Mahalanobis,[2] for Manhattan and [3] for Euclidean:

$$Distance = \sqrt{(X_i - Y_j)^T C^{-1}(X_i + Y_j)} \quad [1]$$

X_i and Y_j are column vectors for objects i and j while C is the covariance matrix.

$$Distance = \sum_{i=1}^p |X_i - Y_i| \quad [2]$$

Where X_i and Y_i are vectors.

$$Distance = \sqrt{(X_1 - Y_1)^2 + (X_2 - Y_2)^2 + \dots + (X_n - Y_n)^2} \quad [3]$$

Where X_n and Y_n are the n^{th} dimensional coordinates of sample X and Y.

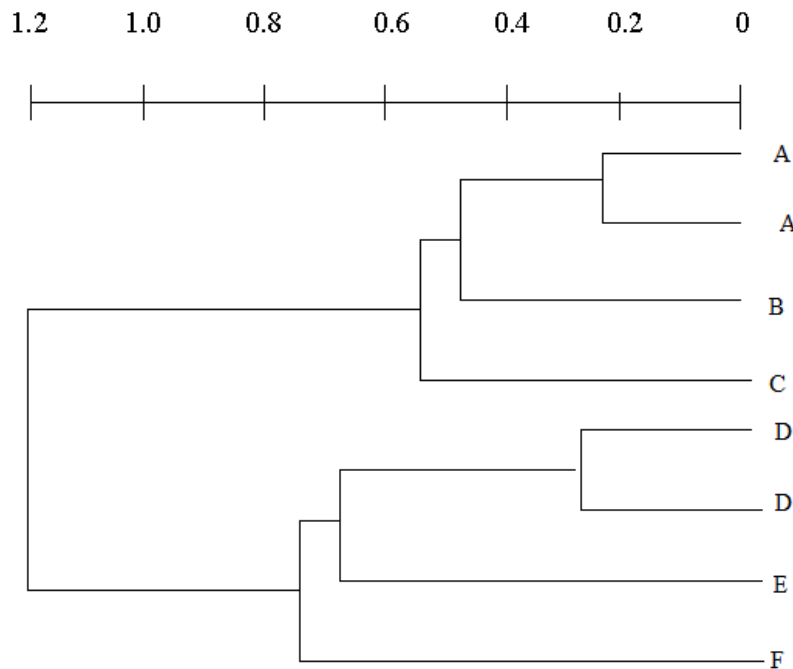


Figure 9 Example of a dendrogram (Taken from Santos et al. , 2004)

Samples that belong to group A has a distance 0.2 from each other. Sample B is distanced 0.5 from the cluster. The distance value may change with the method used for calculation (Santos et al., 2004) (Figure 9).

Principal Component Analysis

Using few axes in the row plot, PCA presents the distances between the points. Aim is to find similarities and differences between these samples. In the Figure 10, PC1 and PC2 is used. PC1 represents the major points while PC2 represents the remaining points. Sum of PC percentages are always close to 100% and PCs are always perpendicular to each other (Santos et al., 2004).

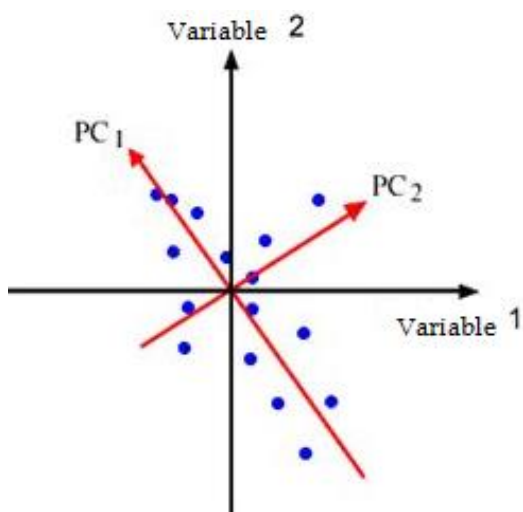


Figure 10 Clustering by PCA (Taken by Santos et al. ,2004)

Qualitative Analysis

There are three main parameters that were calculated from infrared spectra which are band area, bandwidth and frequency values.

Band Area Analysis

Band area can be calculated from smoothed and baseline corrected spectra which gives concentration information. Also, ratios of these band areas can be examined to determine the changes in relative concentrations (Genc, 2014).

Bandwidth Analysis

Bandwidth values are calculated by taking 80% of the height of the signal which gives the dynamic information about the biomolecules. As an example, for the C-H region, bandwidth alterations gives membrane fluidity information while in protein region it gives information about overall protein mobility (Genc, 2014).

Frequency Analysis

The wavenumber value that corresponds to the center of weight and shifts in position provides structural information about biomolecules (Genc, 2014)

1.4 Aim of the Study

Colon cancer is the one of the most significant cause of death in the western countries. Every year, 492,000 people die because of the colorectal cancer while 945,000 people added as estimated new case. In men, it is the third most common

cancer after lung and prostate cancer. In women, it is the third most common cancer after breast and gynecological cancers. (Genç, 2014)

There are many studies that investigate the effect of NaBt and other HDACi inhibitors in genetic level while there is a need for new studies for elucidating structural and functional alterations occurred in cancer cells. For this reason, this study was aimed to investigate the therapeutic effect of NaBt in structural and functional level with the use of ATR-FTIR spectroscopy based on spectroscopic and unsupervised chemometric analysis.



CHAPTER II

MATERIAL AND METHODS

2.1 Cell Culture and Growing Conditions

Caco-2, the human epithelial colorectal adenocarcinoma cells were purchased from ŞAP Enstitüsü (Ankara, Turkey) and kept according to the ATCC guidelines. They were grown in Eagle's minimum essential medium including 1.5 g/L sodium bicarbonate, 1 mM sodium pyruvate, 12 mM L-glutamine, 0.1 mM non-essential amino acids, 20 % FBS and 1 % penicillin-streptomycin. Growing cells were kept at 37°C in a 5% CO₂/95% air atmosphere.

2.2 Sodium Butyrate Treatments

100 mM Sodium butyrate (Sigma, B5887) stock solution was freshly prepared by dissolving in tissue culture grade PBS and stored at +4°C up to 1 week. Cells at 75-80% confluency were treated with 3 mM, 6mM and 9mM sodium butyrate and cultured for 12 h, 24h and 48h.

2.3 ATR-FTIR Spectroscopic Study

2.3.1 Sample Preparation

Control and sodium butyrate treated cells were grown and harvested at 6 independent times.

For ATR-FTIR experiments, cell pellet was obtained by through growing cells until proper consistency which is 75-80%. Cells were trypsinized from the T-75 flasks and their number was determined by using a hemacytometer. Control and treated cells were taken and centrifuged at 100g for 5 minutes. After taking away the cell medium, 6 ml PBS was added onto each pellet and centrifuged again under same conditions. Finally, cell pellet was resuspended with 10 μ l 0.9% PBS solution and this suspension was used as a sample for ATR-FTIR experiments.

2.3.2 Data Acquisition

The one-bounce ATR mode in a Spectrum 100 FTIR spectrometer (Perkin-Elmer Inc., Norwalk, CT, USA) equipped with a Universal ATR accessory were used for the collection of the IR spectra of the cells. To check the consistency of the sample spectra, 3 technical replicates of each independent sample in the studied groups were used. Basically 2 million cells/ technical replicate was directly put on the ATR crystal. To remove unbound water from the sample, it was dried with mild N_2 gas with a constant flow. Spectra of each sample were collected at 4 cm^{-1} resolution, 50 scans, in the 4000-650 cm^{-1} spectral region.

2.3.3 Spectral Data Analysis

Spectral data analysis has been done by using OPUS 5.5 software (Bruker Optics, GmbH). The second order derivative spectra were used for discriminating superimposed and unresolved IR bands. Absorption maximums become minima in the second derivative, therefore, minimum positions were taken as IR peaks. To conclude, in order to make the band *intensity*, bandwidth and frequency analysis; the second derivative order of the cell spectra were taken and subsequently vector normalized in two IR regions (3050–2800 cm^{-1} , 1800– 800 cm^{-1}).

2.3.4 Chemometric Analysis

Discrimination based on spectral alterations between control and Sodium Butyrate-treated cell groups were made by performing Hierarchical cluster analysis (HCA) and Principal Component Analysis (PCA).

For both HCA and PCA, Unscrambler X 10.3 (Camo Software AS) has been used. For HCA, second derivative vector normalized spectra at 4000-650 cm^{-1} spectral region was used. Pearson's correlation coefficients were used for calculating the spectral distances between spectral pairs. Dendrogram was constructed by using Ward's algorithm and the separation between control and treated groups was based on Euclidean distances.

For PCA, like HCA, second derivative vector normalized spectra at 4000-650 cm^{-1} spectral region was used. Discrimination between the control and treated groups was shown as score plots. The origin of the discrimination in terms of spectral variations between groups was demonstrated in loading plots.

2.4 Statistical Data Analysis

The mean was calculated from 6 independent FTIR spectra for this research. Results were given with the mean standard error. To evaluate the statistical significance of the spectral results for control and NaBt treated group, Student-t test was used. Significance was chosen as p values equal to or less than 0.05 for differentiation of the results of sodium butyrate treated group from the control group. Significance degree was denoted as* $p < 0.05$, ** $p < 0.01$, *** $p < 0.001$ and **** $p < 0.0001$.



CHAPTER III

RESULTS AND DISCUSSION

Sodium butyrate, a histone deacetylase inhibitor, has been demonstrated that it induces changes in gene expression, induction of apoptosis, cell cycle arrest, and inhibition of angiogenesis and metastasis in multiple cancers by causing in alterations in acetylation status of chromatin and other non-histone proteins (Ma et al., 2009; Rajendran et al., 2011; Chopin et al., 2009; Giuliano et al., 1999). Therefore, sodium butyrate, alone or in combination with other anti-cancer drugs and radiation treatments, could be used to treat a number of malignant tumors (Kim et al., 2011; Wagner et al., 2010; Medina et al., 1998; Kuefer et al. 2004). Although there are several studies to unravel the therapeutic potential mechanisms of this drug at genetic level (Davie, 2003; Rada-Iglesias et al., 2004 ;Li et al., 2015) its exact mechanism is still unclear and the clinical utility of sodium butyrate is restricted. Therefore this work was conducted to clarify the action/therapeutic potential mechanisms of sodium butyrate in colon cancer (Caco2 cell line) at molecular level using ATR-FTIR spectroscopy, quantitative spectral and chemometric analyses. The 3mM, 6mM and 9mM doses of sodium butyrate were chosen based on previous studies (Shadan et al., 1994; Fukushima et al., 1998; Poorter et al., 2007). These doses were applied to Caco2 cell line for 12h, 24h and 48 h.

3.1 Characterization of Sodium Butyrate Induced-Molecular Alterations in Colon Cancer Cells

3.1.1 ATR-FTIR Spectroscopy

3.1.1.1 Spectral Analysis

To unravel the action mechanism of sodium butyrate on biochemical make up of colon cancer cells, quantitative spectral analysis including band wavenumber, area and bandwidth calculations were done in three different spectral regions: 3030–2800,

1800–1480 and 1480–900 cm^{-1} . The representative spectrum of control Caco2 cells was given Figure 11. As can be seen this figure, this spectrum includes many bands associated with the lipids, proteins, polysaccharides and nucleic acids. The characteristic frequency values and detailed assignments of these bands were given in Table 3.

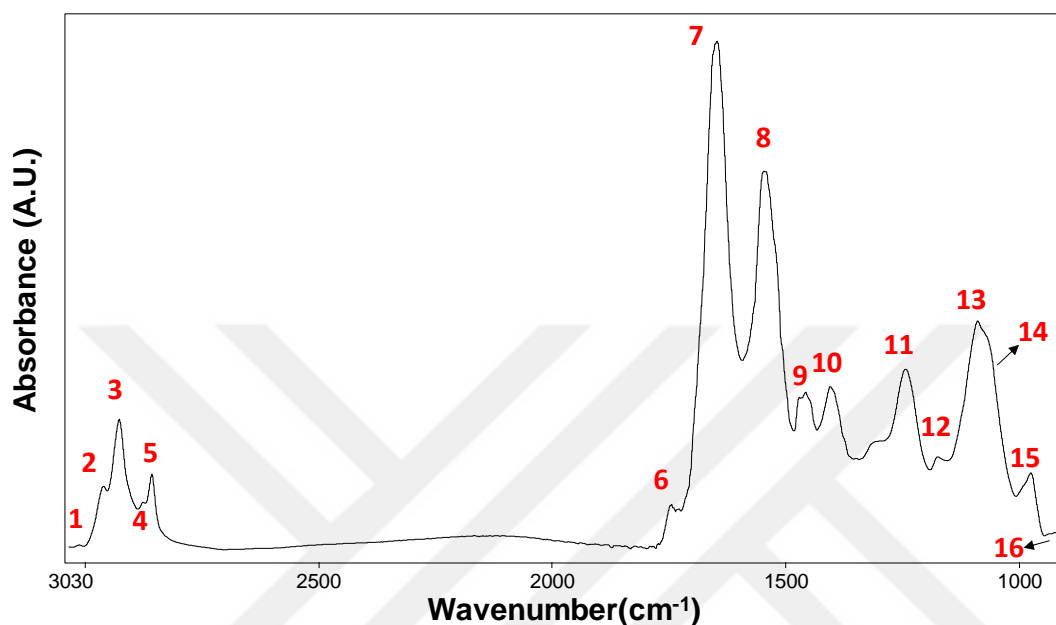


Figure 11 The representantive spectra of control Caco2 cells in the 3030-900 cm^{-1} spectral region.

Table 3 Band assignments of major absorptions in IR spectra of colon cancer cell in the 3030–900 cm^{-1} region based on literature (Choo et al., 1995, Jackson et al., 1998, Banyay et al., 2003, Ramesh et al., 2002, Mourant et al., 2003, Salman et al., 2001, Diem e

Peak no.	Wavenumber (cm^{-1})	Definition of the spectral assignment
1	3008	Olefinic=CH stretching vibration: unsaturated lipids,
2	2958	CH ₃ antisymmetric stretching: lipids, protein side chains, with some contribution from carbohydrates and nucleic acids
3	2921	CH ₂ antisymmetric stretching: mainly lipids, with the little contribution from proteins, carbohydrates, nucleic acids
4	2870	CH ₃ symmetric stretching: protein side chains, lipids, with some contribution from carbohydrates and nucleic acids
5	2851	CH ₂ symmetric stretching: mainly lipids, with the little contribution from proteins, carbohydrates, nucleic acids
6	1740-1744	Ester C=O stretch: triglycerides, cholesterol esters
7	1651	Amide I: (mainly protein C=O stretching), α -helical
8	1546	Amide II: (protein N–H bending, C–N stretching), α -helical structure
9	1468	CH ₂ scissoring: lipids
10	1400	COO ⁻ symmetric stretching: fatty acids
11	1238	PO ₂ ⁻ antisymmetric stretching, fully hydrogen-bonded: mainly nucleic acids with the little contribution from phospholipids
12	1171	CO–O–C asymmetric stretching: ester bonds in cholesteryl esters
13	1084	PO ₂ ⁻ symmetric stretching: nucleic acids and phospholipids
14	1045-1050	C–O stretching: polysaccharides (glycogen)
15	968	C–N [±] –C stretch: nucleic acids, ribose-phosphate main chain vibrations of RNA-DNA
16	915	Ribose ring vibrations:RNA/DNA

3.1.1.1.1. Lipids

NaBt induced-changes in lipid constituents of the cells were determined from the analysis of spectral bands located between 3030–2800 cm^{-1} spectral region. This region is called C–H stretching region and includes several spectral bands which are due to the olefinic (=CH), CH_2 and CH_3 stretching groups. The representative spectra of control, 3mM NaBt treated cells for 12h, 24h and 48h durations at this region were demonstrated in Figure 12, which is used to obtain information about unsaturated lipids (Krishnakumar et al., 2009, Gasper et al., 2009, Severcan et al., 2005). Moreover, this band can be used to monitor lipid peroxidation (Krishnakumar et al., 2009, Leskovjan et al., 2010, Kinder and JM Wessels, 1997, Gasper et al., 2009, Severcan et al., 2005). The band area results of the olefinic band for 3mM, 6mM and 9mM NaBt treatments were given Figure 13A,B and C, respectively. A significant increase in the band area was found for 3mM, 6 mM NaBt treated cells with respect to control ones. Moreover, a more profound increase in the band area of this band was obtained for 48h NaBt treatment in comparison to the 12h and 24h NaBt treatments. These increases may be due to the increased amount of lipid peroxidation end products, containing a =CH group. The increased olefinic band area due to the increased lipid peroxidation end products has been demonstrated previously by Severcan et al. (2005). The reason of this increase may be the compensation for the loss of unsaturation by the presence of =CH groups in lipid peroxidation end-products such as lipid aldehydes and alkyl radicals (Yin. et. al., 2011; Liu et. al., 2002 and 2005). Therefore, the increase in the olefinic band area was obtained instead of a decline in this parameter due to the lipid peroxidation end products (Severcan et. al., 2005).

The increased in lipid peroxidation might be due to NaBt-induced ROS formation in cells since ROS attacks the double bonds of unsaturated fatty acids, which can undergo peroxidation through a chain of oxidative reactions. The enhanced ROS production by NaBt treatment in hepatic and colon cancer cells was demonstrated in previous studies. (Pant et. al. 2017; Tailor et. al, 2014). Tailor et al., states that NaBt mediated apoptosis potentially involves mitochondria-mediated apoptotic pathway. They determined the mitochondria-mediated reactive oxygen species (ROS) generation by MitoSOX which can detect mitochondrial superoxides which can be an indirect marker of hypoxia. In their study, 2.5Mm of NaBt treatment for 24h

showed that 5 fold increase in mitochondrial superoxide/ROS production in SW480 cells and 2 fold increase in HCT-116 cells (Tailor et al.,2014). Moreover, the increased lipid peroxidation in colon cancer cells by NaBt treatment was indicated by Hossain and his colleagues (2004), confirming our results. It has been reported that an increased lipid peroxidation inhibits cellular growth (Morisaki et al., 1982). The growth inhibition in colon cancer cells due to the increased lipid peroxidation was also demonstrated (Hossain et.al., 2004). Therefore, the increased lipid peroxidation by NaBt treatment can alter the growth profile of Caco2 cell lines.

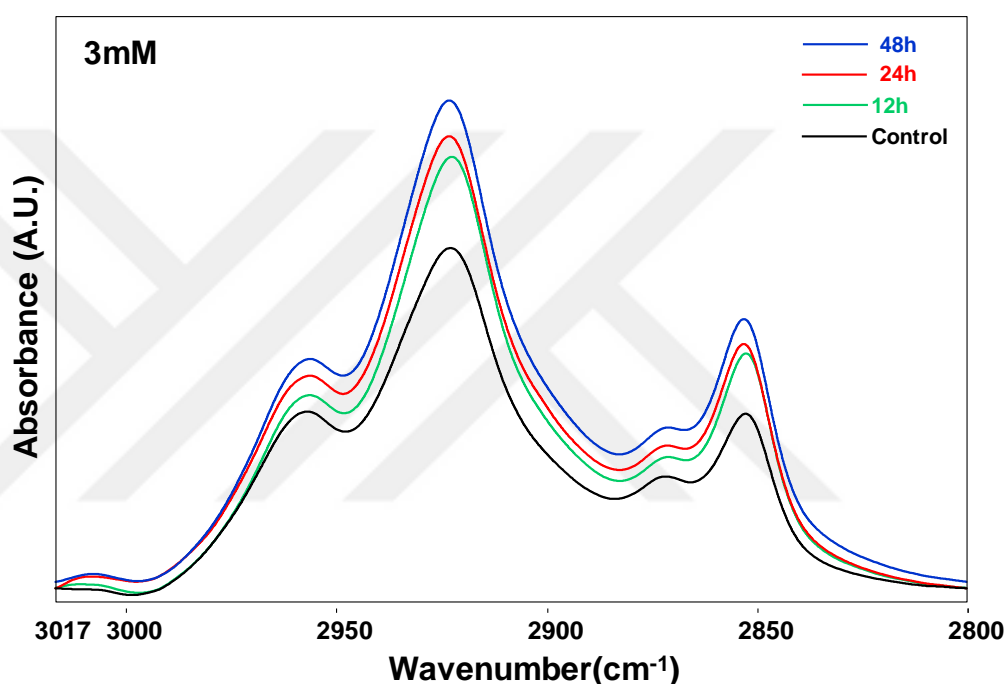


Figure 12 The representative spectra of control and 3mM NaBt treated Caco2 cells for 12h, 24h and 48h in the 3017-2800 cm⁻¹ spectral region.

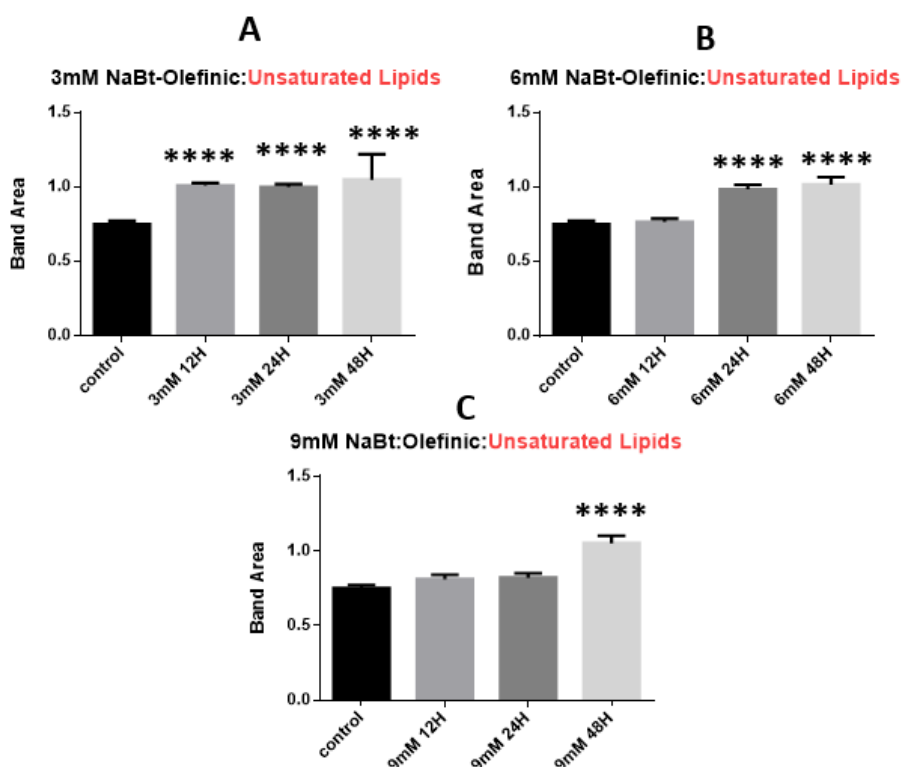


Figure 13 Band area of olefinic band ($3008\text{-}3015\text{ cm}^{-1}$) in control and 3mM NaBt treated (A), control and 6mM NaBt treated (B) control and 9mM NaBt (C) treated Caco2 cells for 12h,24h and 48h.

In addition to unsaturated lipids, to elucidate the alterations in the structure, function and amount of lipids induced by NaBt treatment, lipid associated bands such as CH_2 antisymmetric and symmetric stretching bands were analyzed (Gasper et al., 2009, Severcan et al., 2005, Turker et al., 2014a, Ozek et al., 2014). The band area values of CH_2 antisymmetric stretching bands for control, 3,6 and 9 mM NaBt treated colon cancer cells at 24, 48 and 72h were given in Figure 14 A,B and C. A significant increase in the band area value of this band was obtained for 48h-3mM NaBt treatment. On the other hand, a significant decrease in this value was acquired for 6 and 9 mM NaBt treatment at 12h. At 48h, the increased band area value of this band was obtained for 6 and 9 mM NaBt treatment. The increased lipid amount may be due to the increased lipid biosynthesis. The increased amount of lipid in Caco2 cells with 20mM NaBt treatment was demonstrated in a previous study (Marcil et.al., 2002), confirming our findings. On the other hand, the decreased concentration of lipids may be due to the increased lipid degradation due to

the increase in the lipid peroxidation (Ozek et al., 2014).

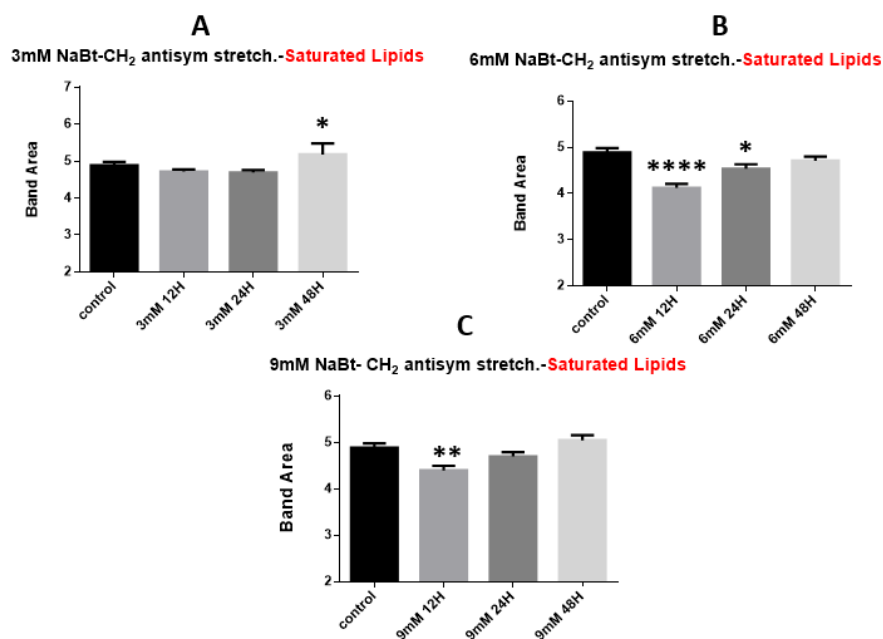


Figure 14 Band area of CH₂ antisymmetric stretching bands (2921-2851 cm⁻¹) in control and 3mM NaBt treated (A), control and 6mM NaBt treated (B) control and 9mM NaBt (C) treated Caco2 cells at 12h,24h and 48h.

In order to understand the alteration in the membrane fluidity/dynamics of the colon cancer cells with NaBt treatment, the bandwidths of the CH₂ antisymmetric stretching band were measured (Turker et al., 2014a, Ozek et al., 2014, Cakmak et al., 2006). A significant increase in this parameter was obtained with NaBt treatment for all doses, implying the increase in the membrane fluidity (Figure 15 A, B, and C). Normally, membranes in cancer cells have more fluidity than the normal cells because higher membrane fluidity closely relates to proliferation, metastatic ability and invasive potential of cancer. The increased membrane fluidity in K562 cells with NaBt treatment was previously shown, supporting our results (Nathan et. al., 1998). Nathan et al., stated that different concentrations of NaBt affect membrane fluidity differently. They reported that higher dose of NaBt affects the cells adversely, leading to an increase in fluidity. This increase is associated with the changes in the composition of membrane lipids like cholesterol and phospholipid and their ratios amounts (Nathan et. al., 1998). Our results also showed an increase in the cholesterol esters and triacylglycerols amounts in NaBt treated cells

(**Figure 17**).

In addition to this parameter, membrane-lipid order (acyl chain flexibility) of cancer cells, the shifts in the band position of the same band calculated (Turker et al., 2014a, Ozek et al., 2014) since the correlation between the lipid order and the membrane fluidity is quite important for regulating the proper functioning of the cells (Boesze-Battaglia and Schimmel, 1997). The wavenumber calculations for control and NaBt treated cells were given in Figure 16 A, B and C. A shift in the frequency of this band to higher values was obtained with NaBt treatment, indicating an increase in the number gauche conformers of lipid molecules which reveals a decrease in lipid order (Severcan, 1997). The relationship between lipid order, fluidity and cell physiology is well established. The changes in these parameters affect many processes associated with cell growth, differentiation, and cellular function (Parola,1993). Therefore, the anti-proliferative effects of NaBt on cancer cell is related to the changes in the membrane order and dynamics.

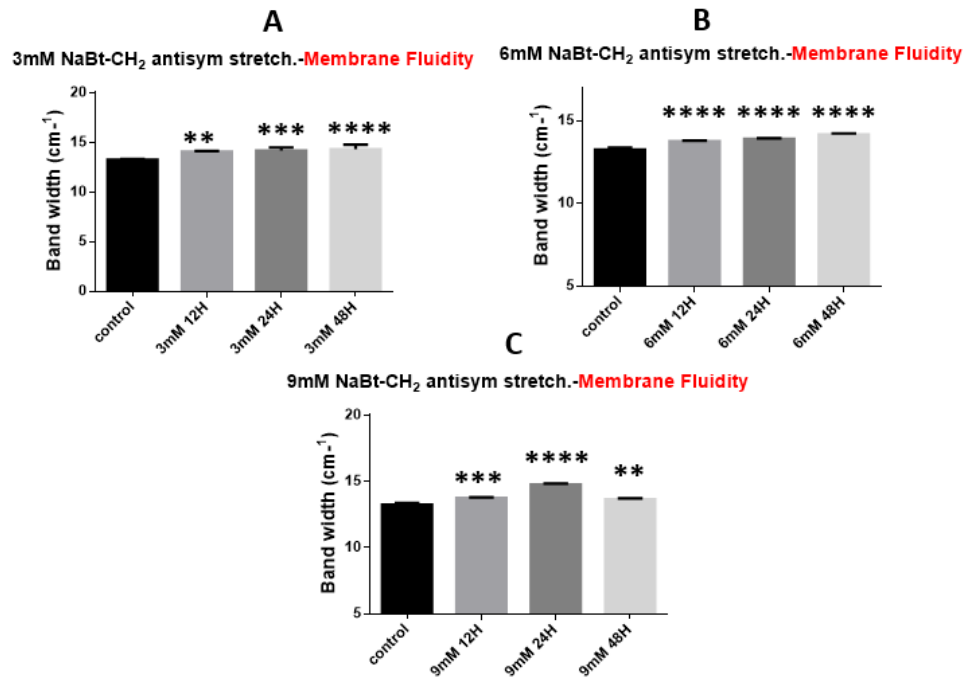


Figure 15 Band width of CH₂ antisymmetric stretching band (2921cm⁻¹) in control and 3mM NaBt treated (A), control and 6mM NaBt treated (B) control and 9mM NaBt treated (C) Caco2 cells at 12h,24h and 48h.

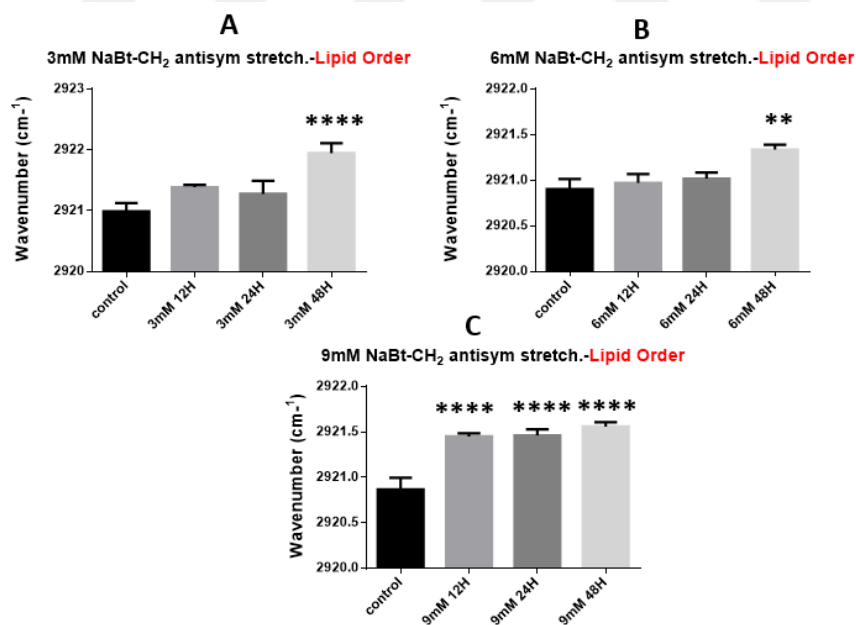


Figure 16 Wavenumber of CH₂ antisymmetric stretching band (2921cm⁻¹) in control and 3mM NaBt treated(A), control and 6mM NaBt treated (B) control and 9mM NaBt treated(C) Caco2 cells at 12h,24h and 48h.

The changes in the cholesterol esters and triacylglycerols within the colon

cancer cells induced by NaBt treatment, ester C=O stretching band at 1740 cm^{-1} was analyzed. The band area measurements of this band were given in Figure 17. NaBt treatment increased the band area of this band, indicating increased amount of cellular triacylglycerols and cholesterol esters (Nara et al., 2002). Significant elevation of triacylglycerol content in Caco2 cells with NaBt treatment was shown by Marcil et.al. (2002) which verifies our result.

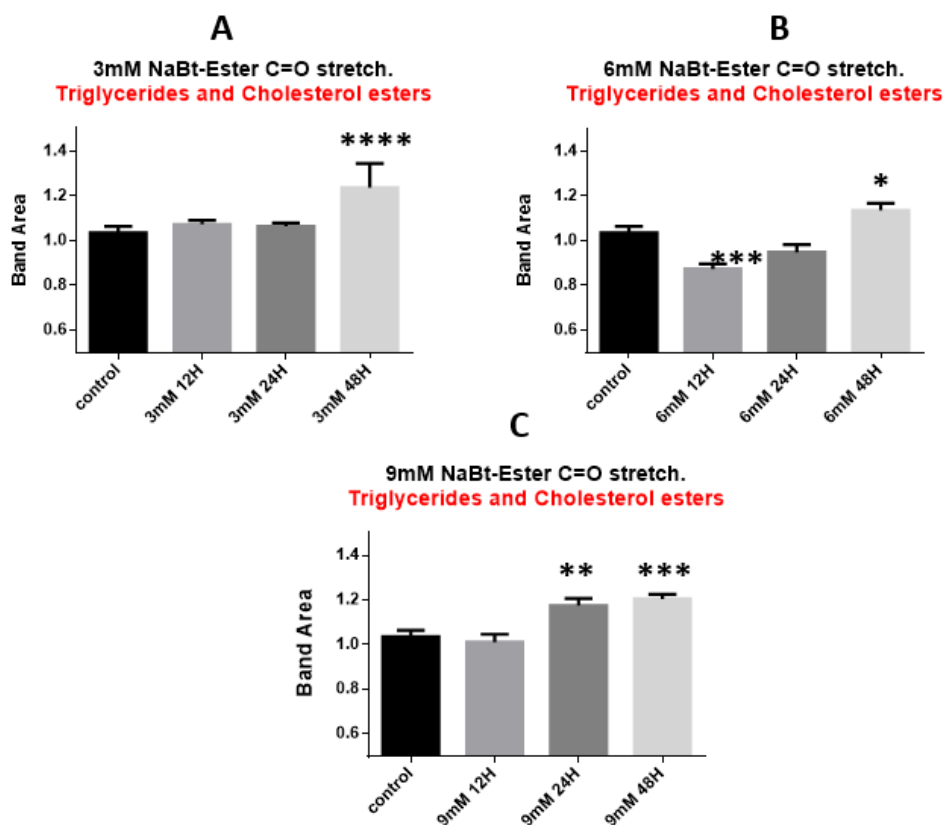


Figure 17 Band area of Ester C=O stretching band (1740 cm^{-1}) for control and 3mM NaBt (A), control and 6mM NaBt (B) control and 9mM NaBt (C) treated Caco2 cells at 12h,24h and 48h.

3.1.1.1.2 Proteins

To elucidate the changes in contextual alterations in Caco2 cells by NaBt treatment, the band area of Amide I (1651 cm^{-1} : of α -helix) was calculated (Hata! Başvuru kaynağı bulunamadı.20). (Severcan and Haris, 2012, Turker et al., 2014b, Turker et al., 2014a, Ozek et al., 2014, Cakmak et al., 2006). Figure 20 A, B and C demonstrated the band area of Amide I bands for control-3mM NaBt, control- 6mM

NaBt and control-9mM NaBt treated Caco2 cells for 12h, 24h and 48h. A significant decrease in protein concentration was obtained in only 12h and 24 h NaBt treated cells for 3mM dose with respect to the control ones while the significant diminish in protein amount was observed in 12h, 24h and 48h NaBt treated cells for 6mM and 9mM doses. This decline can be due to increased protein degradation or diminish in protein synthesis. Increased protein degradation can be due to enhanced ROS production by NaBt since ROS induced-oxidative damages in protein is very well known. Moreover, the upregulation of various components of the ubiquitin-proteasome systems in colon cancer cells due to NaBt treatment was demonstrated in previous studies (Tan et.al., 2002; Tong et. al., 2008), implying an increase in proteolysis i.e. protein degradation because of NaBt treatment, which confirms our findings. The decreased protein synthesis can be supported by the decrease in RNA and nucleic acid content in NaBt treated cells.

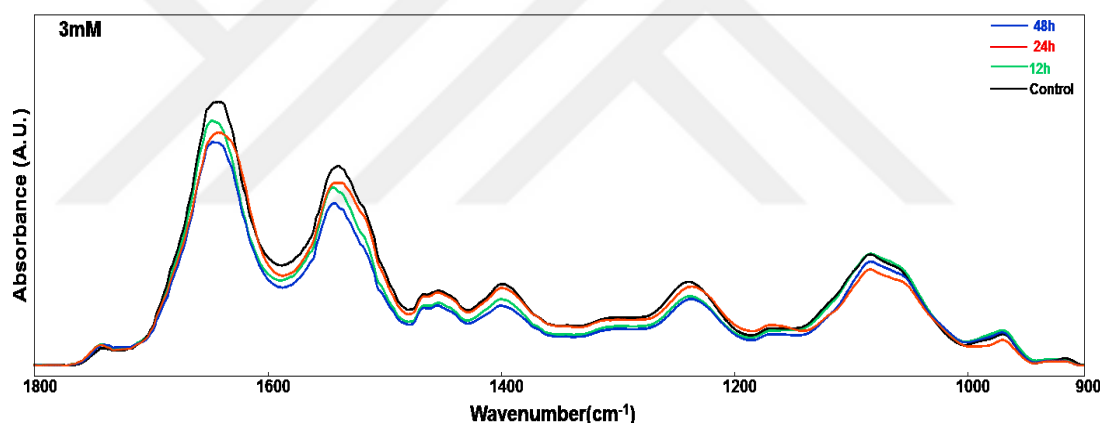


Figure 18 The representative spectra of control and 3mM NaBt treated Caco2 cells for 12h, 24h and 48h in the 1800-900 cm^{-1} spectral region.

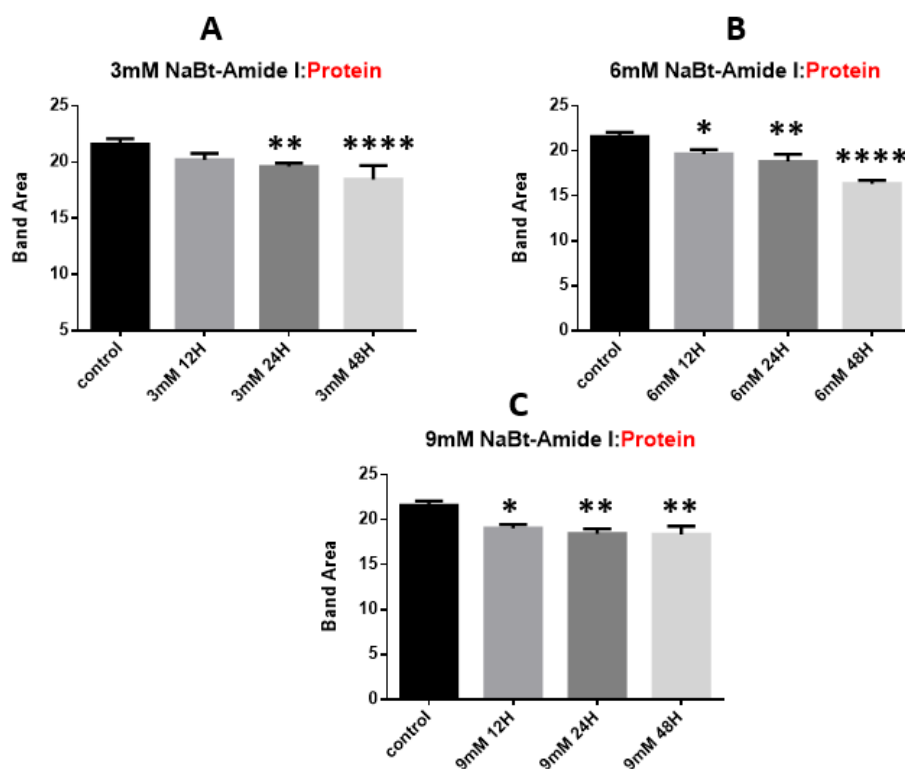


Figure 19 Band area of Amide I band (1651cm⁻¹) in control and 3mM NaBt treated(A), control and 6mM NaBt treated (B) control and 9mM NaBt treated (C) Caco2 cells at 12h, 24h and 48h .

3.1.1.1.3 Nucleic Acids

To determine the alterations in nucleic acid content due to NaBt treatment, the bands at 1238 cm⁻¹ and 1084 cm⁻¹ originating from PO₂⁻ antisymmetric and symmetric vibrations of nucleic acids were analyzed (19). Significant reduction in the band area values of these bands was found in the NaBt treated cells (Figure 20 A,B and C), implying a decline in nucleic acid content in NaBt treated cells cells. Moreover, to identify the alteration in RNA amount, the band area values 915 cm⁻¹ bands was calculated. The significant decreased in this band area was observed with NaBt treatment in all doses, suggesting the diminish in RNA concentration (Figure 21 A,B and C). This decrease may be due a decrease in the synthesis or an increased degradation of nucleic acids (DNA, RNA). Tan and his colleagues demonstrated the reduced expression of proteins role in nucleotide biosynthesis, confirming our findings (Tan et. al., 2008). Moreover, Zeng et. al (2017) demonstrated NaBt induced-DNA fragmentation in HCT116 colon cancer cells, also supports NaBt induced degradation of nucleic acids.

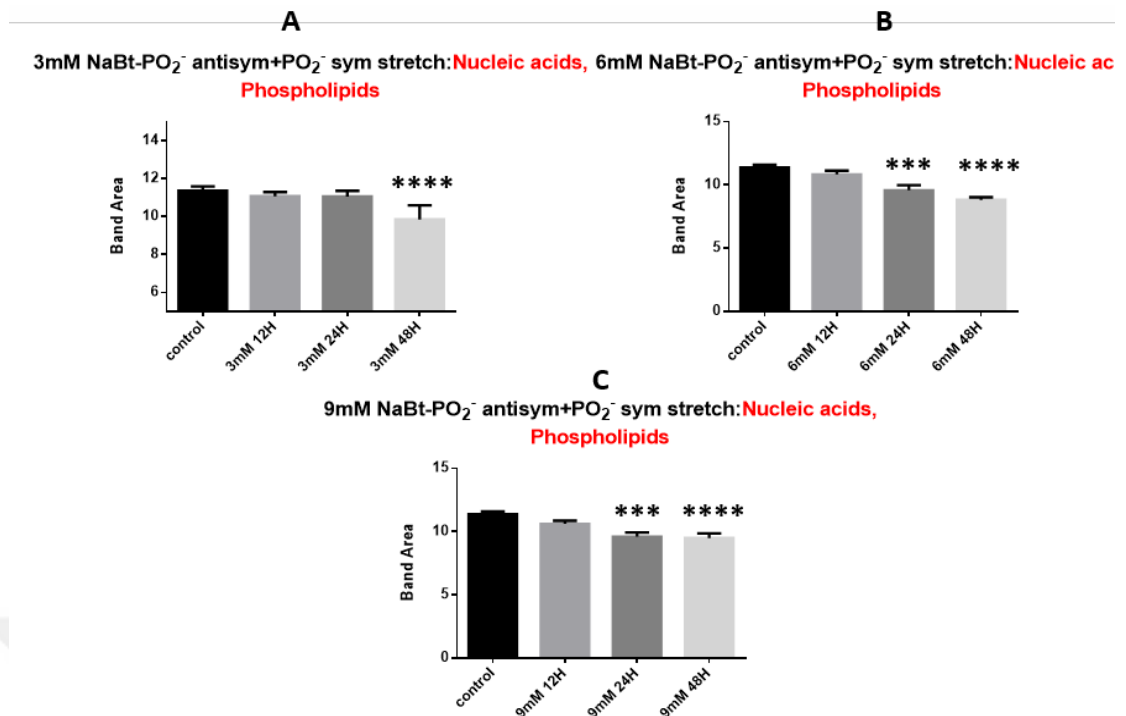


Figure 20 Band area of PO₂⁻ antisymmetric and symmetric bands (1238 cm⁻¹) in control and 3mM NaBt treated (A), control and 6mM NaBt treated (B) control and 9mM NaBt treated (C) Caco2 cells at 12h, 24h and 48h .

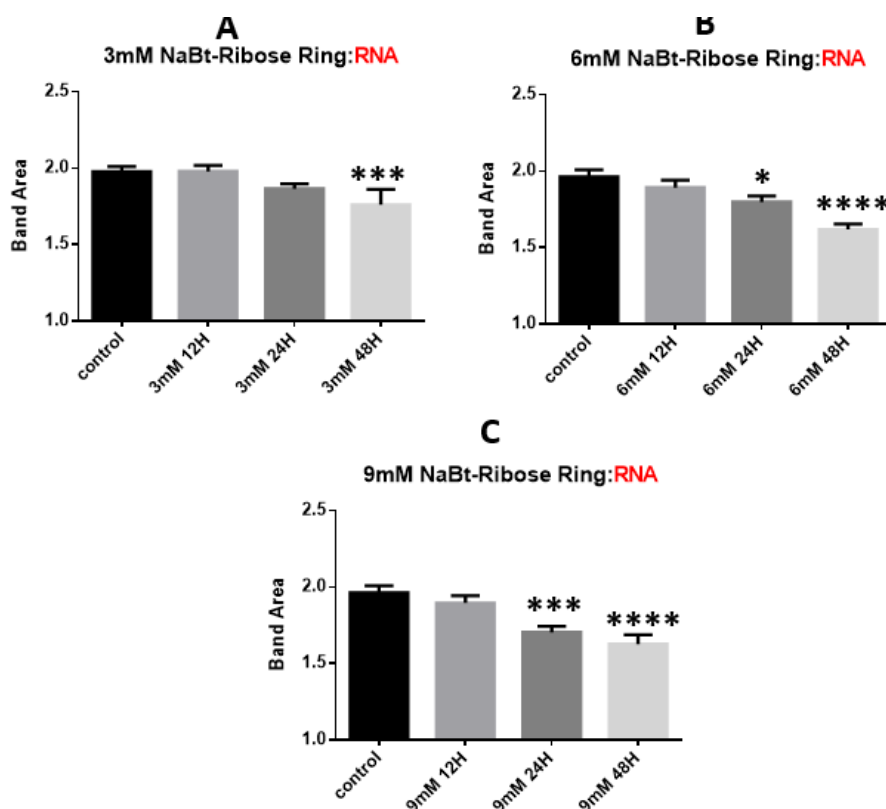


Figure 21 Band area of Ribose Ring: RNA bands (1084 cm^{-1}) in control and 3mM NaBt treated(A), control and 6mM NaBt treated(B) control and 9mM NaBt treated(C) Caco2 cells at 12h, 24h and 48h .

3.1.1.2 Chemometric Analysis

PCA and HCA were performed to control and NaBt treated colon cancer cell spectra to determine the whether there is a clustering between studied groups based on the spectral variances among them. Both chemometric approaches are unsupervised multivariate analysis methods, enabling to identify and differentiate different spectral groups (Gasper et al, 2009). Therefore, it is commonly used to discriminate the different biological systems such as microorganisms, cell, membranes, even tissues.

3.1.1.2.1 Principal Component Analysis (PCA)

PCA is a well-established multivariate analysis method, suited for distinguishing small reoccurring spectral variations in large spectral data sets containing uncorrelated variations. Spectral variations between the sample groups are explained by principal components (PC). PC-1 is the variable, explaining the

variation first best while the PC-2 is the second best and so on. Samples are generally clustered/classified based on these components, which can be clearly seen in PCA score plots since score plots are plotted based on a pair of two score vectors. These plots used to demonstrate the relationships between studied groups of samples. The score plots of control and 3mM NaBt, control and 6mM NaBt at 12,24 and 48h were given in Figure 22 and Figure 23, respectively. For the same plot for control and 9mM NaBt treated cells at same time intervals was demonstrated in Figure 24. As can be seen from these figures, 62% of the total data variances among control, 12h, 24h and 48h treatment groups in the case of 3mM and 9mM NaBt were explained by PC1 and PC2 whereas, 65% of data variances among studied groups in the case of 6mM NaBt were described by PC1 and PC2.

In PCA, loading plots of PCA scores give information about the spectral origin of the variations that differentiate data groups spectrally. Positive score values in the loadings shows the increase in contribution of the signals that are measured in IR spectrum. Likewise, negative score values in the loadings shows the decrease in contribution of the signals (Ozek, 2015). The loading plots of 3mM, 6mM and 9mM doses of NaBt showed in Figures 24,25 and 26. As can be seen from these figures, high loading values for C-H stretching ($3000-2800\text{ cm}^{-1}$) and fingerprint region ($1800-650\text{ cm}^{-1}$) are obtained which indicates the intensity changes within these regions. Both score and loading plots of 3mM, 6mM and 9mM NaBt treatment clearly indicated that all NaBt treated groups were successfully discriminated from control cancer, implying that the biochemical makeup of the studied groups were significantly different from each other.

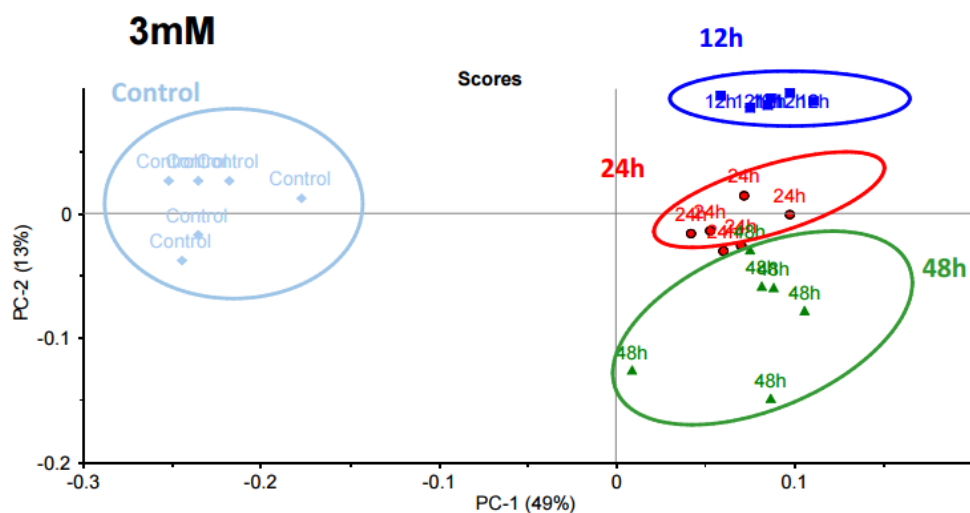


Figure 22 PCA score plots of control, 3mM NaBt treated Caco2 cells at 12h,24h and 48h. PCA was performed with second derivative vector normalized spectra within the 4000-650cm⁻¹ spectral range.

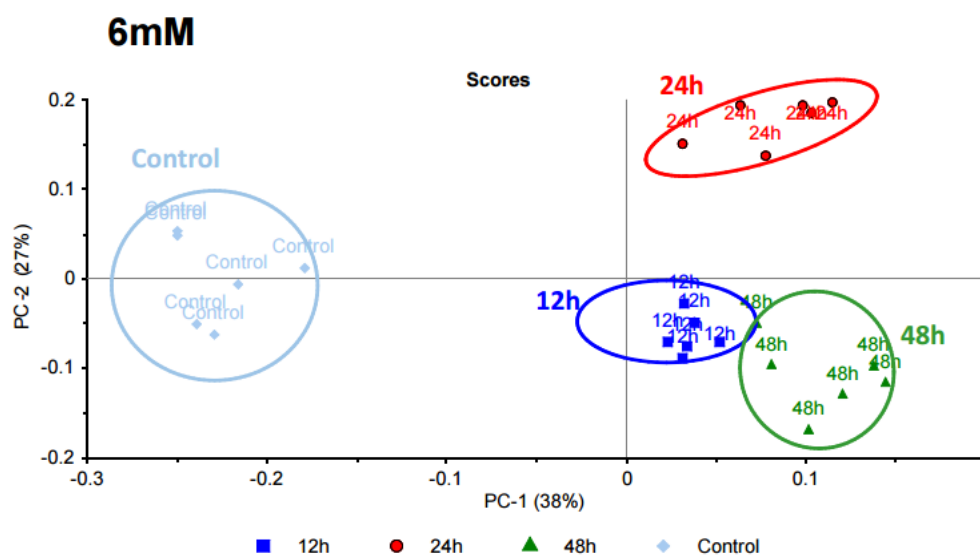


Figure 23 PCA score plots of control, 6mM NaBt treated Caco2 cells at 12h,24h and 48h. PCA was performed with second derivative vector normalized spectra within the 4000-650cm⁻¹ spectral range.

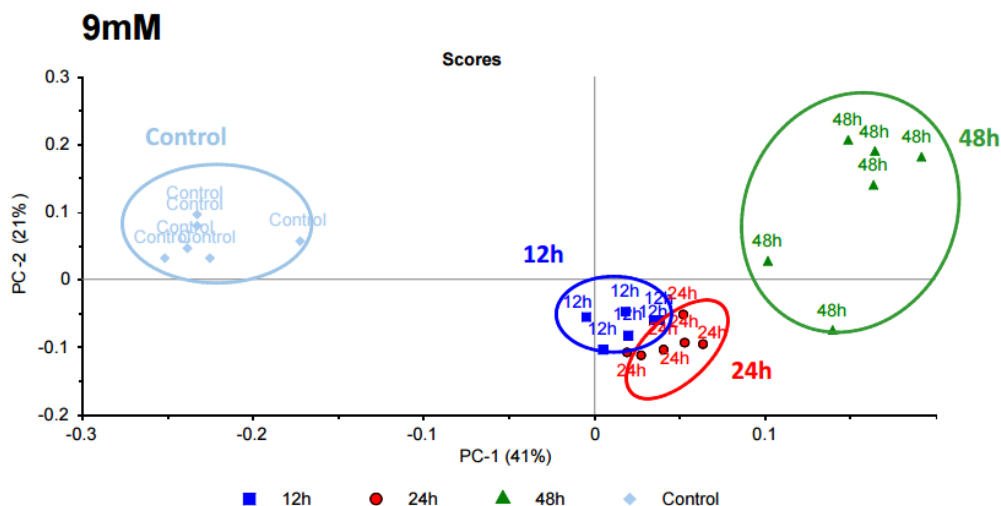


Figure 24 PCA score plots of control, 9mM NaBt treated Caco2 cells at 12h,24h and 48h. PCA was performed with second derivative vector normalized spectra within the 4000-650 cm^{-1} spectral range.

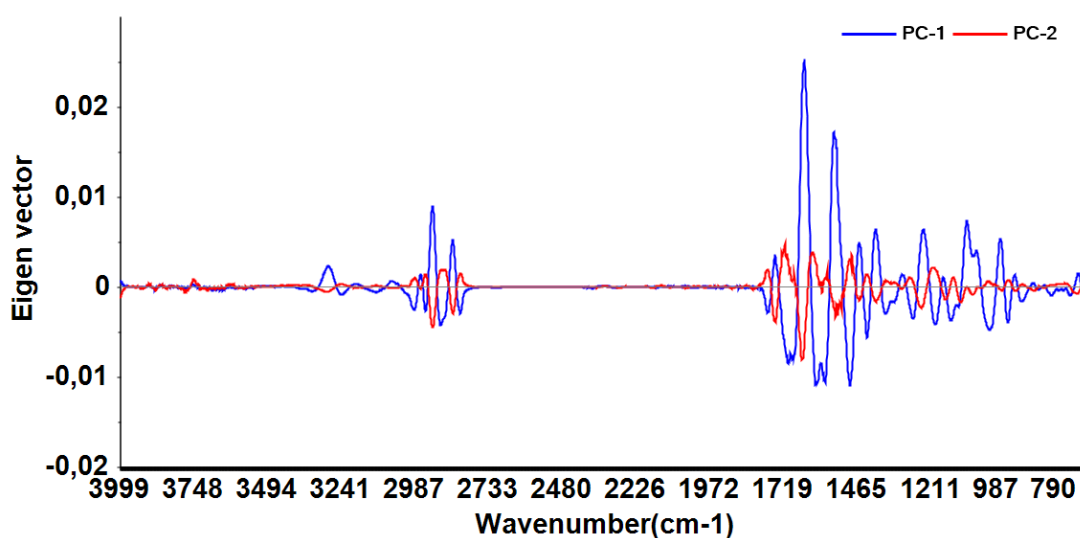


Figure 25 PCA loading plot for 3mM in 4000-650 cm^{-1}

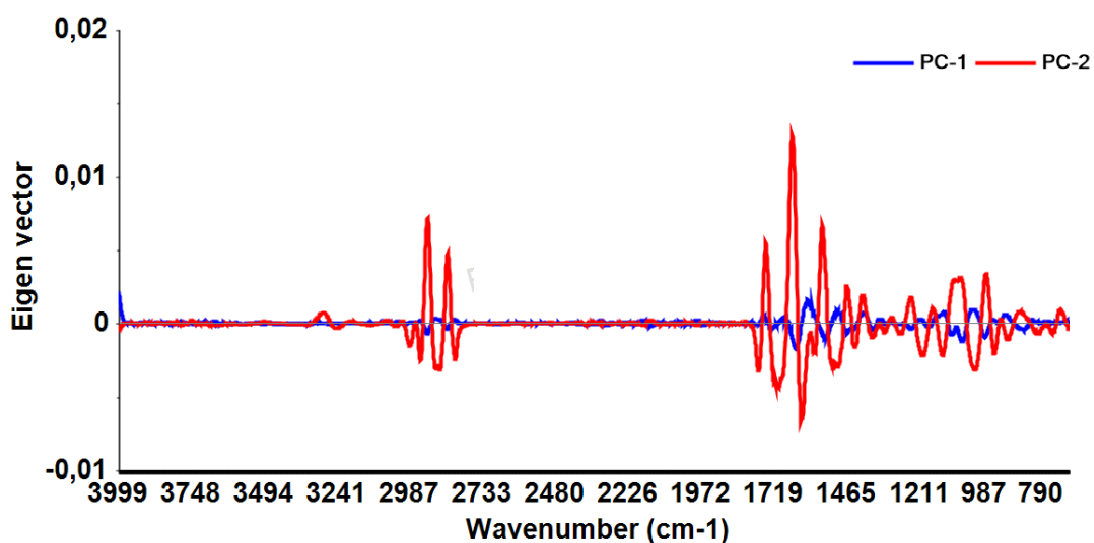


Figure 26 PCA loading plot for 6mM in 4000-650 cm^{-1}

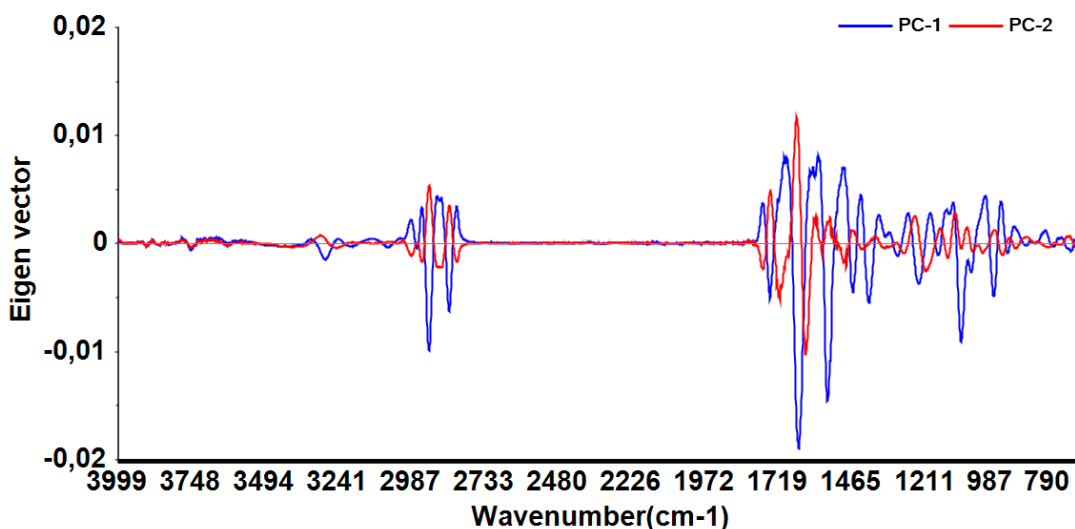


Figure 27 PCA loading plot for 9mM in 4000-650 cm^{-1}

3.1.1.2.2 Hierarchical Cluster Analysis (HCA)

To confirm the successful segregation of studied groups, HCA was employed based on the spectral differences. HCA is generally performed to group samples depending on their characteristics. On the other hand, PCA generally used for to explore general relationships among the data whether the samples show clear differentiation or not. If the differentiation is clear, additional cluster analysis should be conducted. In HCA, groups are clustered and demonstrated as dendrogram. The similarity of samples is

indicated as heterogeneity value in the x axes of dendrogram. Increase in heterogeneity value shows the decrease in similarity index (Wang & Mizaikoff, 2008). Figure 287 and 28 demonstrated the dendrograms of control-12h, 24h and 48h NaBt treated cells for 3mM and 6mM dosed of NaBt, respectively while the same figure for 9mM NaBt was given in Figure 309. As can be inferred from these figures, all groups with high heterogeneity value are clearly clustered as a separate group. All NaBt treated samples of each group was clustered in different branch than non-treated (control) group. This indicated that there was significant alteration in molecular content and structure among control and NaBt treated Caco2 cells in all doses.

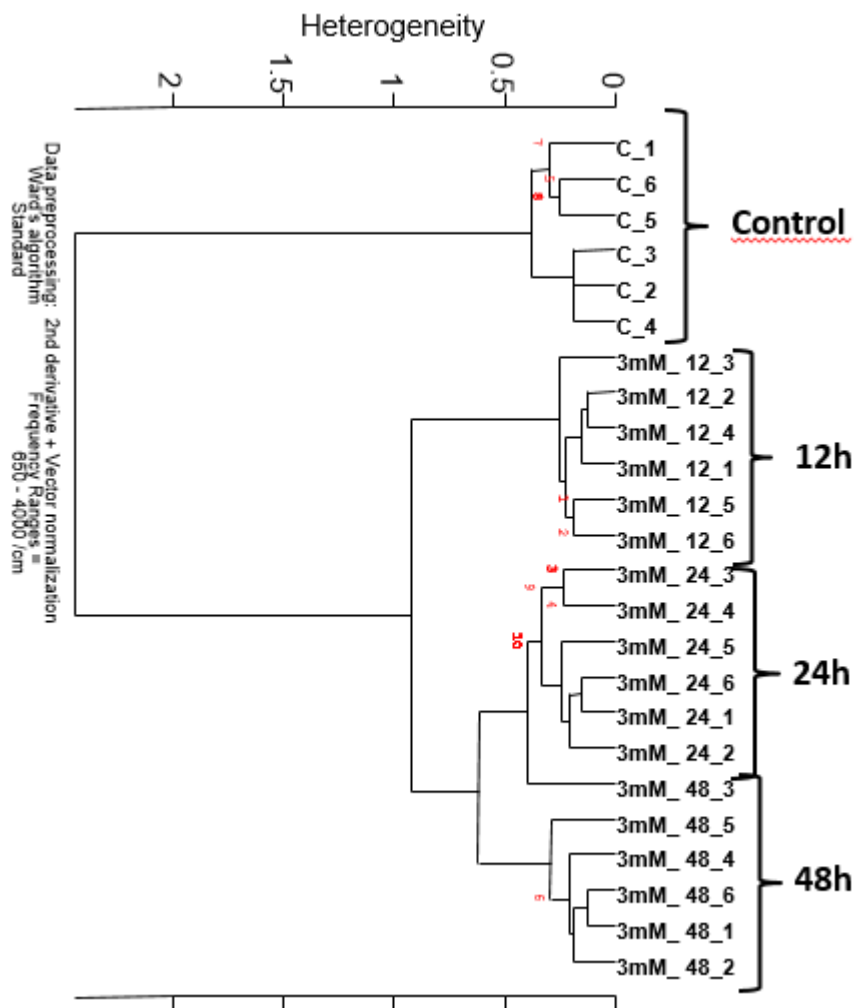


Figure 28 Hierarchical clustering of the 3mM NaBt treated Caco2 cell lines within different time durations as control, 12h,24h and 48h. Clustering was performed using

Ward's algorithm and second derivative vector normalized spectra within the 4000-650cm⁻¹ spectral

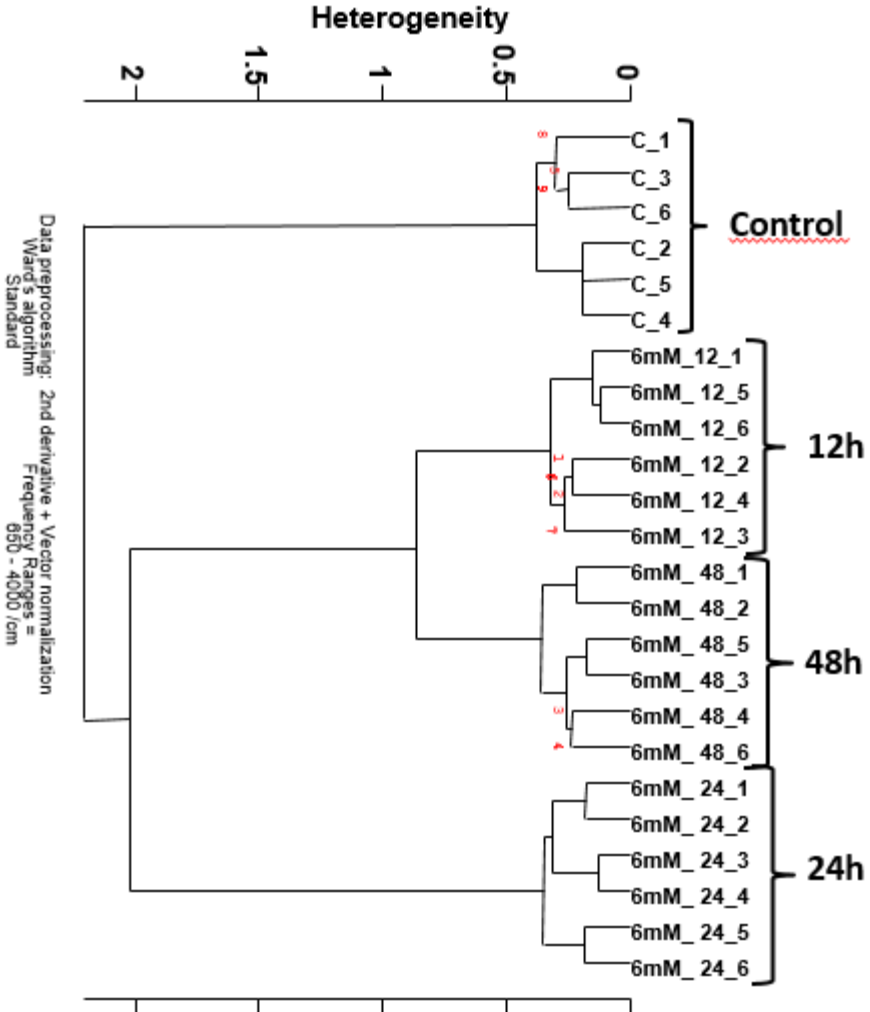


Figure 29 Hierarchical clustering of the 6mM NaBt treated Caco2 cell lines within different time durations as control, 12h,24h and 48h. Clustering was performed using Ward's algorithm and second derivative vector normalized spectra within the 4000-650cm-1 spectra

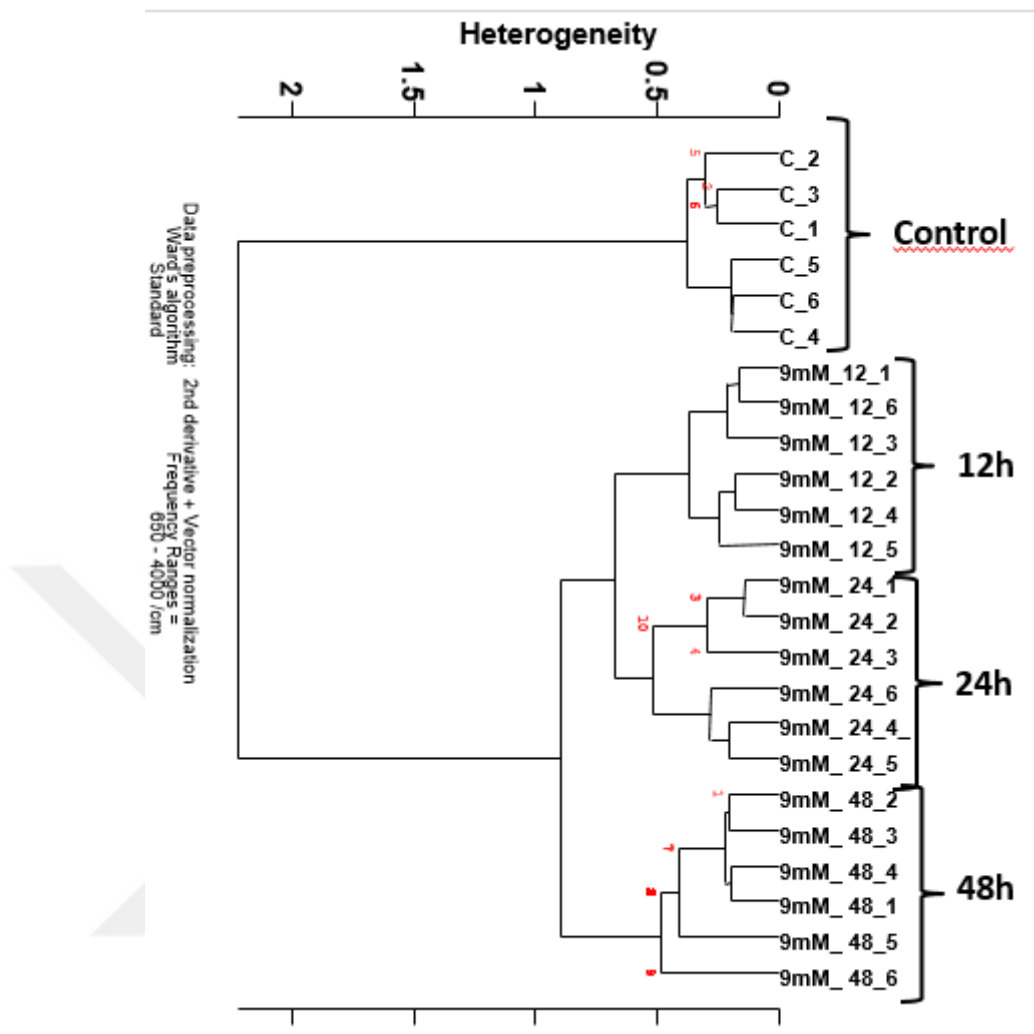


Figure 30 Hierarchical clustering of the 9mM NaBt treated Caco2 cell lines within different time durations as control, 12h,24h and 48h. Clustering was performed using Ward's algorithm and second derivative vector normalized spectra within the 4000-650cm⁻¹ spectral



CHAPTER IV

CONCLUSION

Normal cell growth has been highly associated with the balance between acetylation and deacetylation. Structural alterations cause abnormal cell growth that may lead to cancer. Among the HDACi's, NaBt has a curative potential for colon cancer. NaBt is normally produced in healthy human colon and the rate of butyrate is mostly influenced by diet. Studies (Zeng et al.,2014) showed that major butyrate-producing bacteria *Faecalibacterium prausnitzii* can be affected by dietary xylo-oligosaccharides. In that case, the dietary changes affect the NaBt amount in human colon which reduces the HDAC inhibition that may lead to cancer.

Although several studies have been done for the therapeutic effect of NaBt, exact mechanism at molecular level has not been fully elucidated yet. For this reason, we use ATR-FTIR spectroscopy results coupled with chemometric analysis methods to clarify action/therapeutic potential mechanisms of Sodium Butyrate in Caco2 cell line.

The spectral data analysis of 3008-3015 cm^{-1} band for unsaturated lipids for 3mM, 6mM and 9mM NaBt treated cells has been done. Band area analysis showed that, there is a significant increase in 3mM, 6 mM NaBt treated cells with respect to control ones. In the time domain, 48h NaBt treated cells showed a profound increase with respect to 12h and 24h NaBt treated cells. End products of lipid peroxidation that contains =CH group can be considered as the reason for these results (Severcan et al., 2015) The compensation for the loss of unsaturation by the presence of =CH groups in lipid peroxidation end products such as lipid aldehydes and alkyl radicals may be considered as another reason for this increase (Yin. et. al., 2011; Liu et. al., 2002 and 2005). The increase in lipid peroxidation can be due to the ROS formation induced by NaBt, which are attacking the double bonds of unsaturated fatty acids that can go under peroxidation. In addition, increased lipid peroxidation in colon cancer cells treated by NaBt has been demonstrated by Hossain and his colleagues in

2004 which is confirming our results. Morisaki and his colleagues showed that increase in lipid peroxidation inhibits cellular growth in 1982, which can alter the growth profile of Caco2 cell lines in colon cancer. In order to elucidate the alterations in the amount, function and structure of the lipids induced by NaBt, CH₂ antisymmetric and symmetric stretching bands were analyzed and results showed that band area value increase in 3mM 48h, 6mM 48h and 9mM 48h that may due to increased biosynthesis. Marcil et al. study with 20mM NaBt in 2012 and showed the increased amount of lipids that confirms our study. A significant decrease in the band area value was obtained in 6mM 12h and 9mM 12h that may be due to increased lipid degradation caused by lipid peroxidation (Ozek et al., 2014)

For finding the change in membrane fluidity/dynamics of the colon cancer cells after NaBt treatment, CH₂ antisymmetric stretching can be measured (Turker et al., 2014a, Ozek et al., 2014, Cakmak et al., 2006) and for all doses a significant increase was obtained which can be interpreted as increase in membrane fluidity. The increased membrane fluidity in K562 cells with NaBt treatment was previously shown, supporting our results (Nathan I et. al., 1998). For finfind the change in membrane-lipid order of cancer cells, shifts in the wavenumber of the same band was calculated (Turker et al., 2014a, Ozek et al., 2014). A frequency shift to higher values was obtained with NaBt treatment, means that an increase in the number gauche conformers of lipid molecules which reveals a decrease in lipid order (Severcan, 1997) which affects many processes like cell, growth, differentiation and cellular function (Parola, 1993). Therefore, the anti-proliferative effects of NaBt on cancer cell is related to the changes in the membrane order and dynamics.

Ester C=O stretching band was analyzed for the changes in the cholesterol esters and triacylglycerols induced by NaBt.As verified by Marcil et al. in 2002, NaBt treatment has increased the amount of cellular triacylglycerols and cholesterol esters in our study.

For the proteins, a significant decreased protein concentration was obtained in only 12h and 24h NaBt treated cells for 3mM dose while a significant diminish in protein amount was found in all times of 6mM and 9mM. Protein concentration can be

decreased by increased protein degradation or decreased protein synthesis. Increase protein degradation can be due to ROS production by NaBt, as demonstrated in previous studies (Tan et.al., 2002; Tong et. al., 2008),e upregulation of various components of the ubiquitin-proteasome systems in colon cancer cells due to NaBt treatment implying an increase in proteolysis i.e. protein degradation because of NaBt treatment, which confirms our findings. The decreased protein synthesis can be supported by the decrease in RNA and nucleic acid content in NaBt treated cells.

A significant decrease in the band area values in 915cm⁻¹ bands was calculated which suggests diminish in RNA concentration. This decrease may be due a decrease in the synthesis or an increased degradation of nucleic acids (DNA, RNA). Tan and his colleagues demonstrated the reduced expression of proteins role in nucleotide biosynthesis, confirming our findings (Tan et. al., 2008). Moreover, Zeng et. al (2017) demonstrated NaBt induced-DNA fragmentation in HCT116 colon cancer cells,also supports NaBt induced degradation of nucleic acids.

For the HCA, in all doses all time dependent groups are successfully differentiated from the control group regarding the spectral difference between 4000-650cm⁻¹. PCA's are approved the results in HCA. The same differentiation can be seem for 12h dose dependent HCA and PCA for 3mM, 6 mM and 9 mM.Both spectral data and chemometric analyses indicate there is a theurapeutic effect of NaBt on colon cancer cells. Not only it causes lipid alterations but also indirectly remodelling of biochemical makeup of cell. Animal and clinical studies are required for future studies.



REFERENCES

Ami, D., et al. (2012). "Fourier transform infrared microspectroscopy of complex biological systems: from intact cells to whole organisms." Intrinsically Disordered Protein Analysis: Volume 1, Methods and Experimental Tools: 85-100.

Argov, S., et al. (2002). "Diagnostic potential of Fourier-transform infrared microspectroscopy and advanced computational methods in colon cancer patients." Journal of biomedical optics **7**(2): 248-254.

Baker, M. J., et al. (2014). "Using Fourier transform IR spectroscopy to analyze biological materials." Nature protocols **9**(8): 1771-1791.

Banyay, M., et al. (2003). "A library of IR bands of nucleic acids in solution." Biophysical chemistry **104**(2): 477-488.

Bolden, J. E., et al. (2006). "Anticancer activities of histone deacetylase inhibitors." Nature reviews. Drug discovery **5**(9): 769.

Cakmak, G., et al. (2006). "17 β -Estradiol induced compositional, structural and functional changes in rainbow trout liver, revealed by FT-IR spectroscopy: a comparative study with nonylphenol." Aquatic toxicology **77**(1): 53-63.

Choo, L. P., et al. (1995). "Infrared spectra of human central nervous system tissue: Diagnosis of alzheimer's disease by multivariate analyses." Biospectroscopy **1**(2): 141-148.

Cohenford, M. A. and B. Rigas (1998). "Cytologically normal cells from neoplastic cervical samples display extensive structural abnormalities on IR spectroscopy: implications for tumor biology." Proceedings of the National Academy of Sciences **95**(26): 15327-15332.

Davie, J. R. (2003). "Inhibition of histone deacetylase activity by butyrate." The Journal of nutrition **133**(7): 2485S-2493S.

De Poorter, J. J., et al. (2007). "Optimization of short-term transgene expression by sodium butyrate and ubiquitous chromatin opening elements (UCOEs)." The journal of gene medicine **9**(8): 639-648.

Derenne, A., et al. (2011). "The FTIR spectrum of prostate cancer cells allows the classification of anticancer drugs according to their mode of action." Analyst **136**(6): 1134-1141.

Diem, M., et al. (1999). "Infrared spectroscopy of cells and tissues: shining light onto a novel subject." Applied Spectroscopy **53**(4): 148A-161A.

Dokmanovic, M., et al. (2007). "Histone deacetylase inhibitors: overview and perspectives." Molecular cancer research **5**(10): 981-989.

dos Santos, H. T. L., et al. (2013). Chemometrics: Theory and Application. Multivariate Analysis in Management, Engineering and the Sciences, InTech.

Fukushima, K., et al. (1998). "Sodium butyrate-induced liver-type alkaline phosphatase activity in a small intestinal epithelial cell line, IEC6." Digestive diseases and sciences **43**(5): 1116-1123.

Gasper, R., et al. (2009). "IR spectroscopy as a new tool for evidencing antitumor drug signatures." Biochimica et Biophysica Acta (BBA)-Biomembranes **1788**(6): 1263-1270.

Gasper, R. and E. Goormaghtigh (2010). "Infrared spectroscopy as a new tool for the screening of antitumoral agents inducing original therapeutic action."

Gasper, R., et al. (2009). "It takes two to tango: regulation of G proteins by dimerization." Nature reviews Molecular cell biology **10**(6): 423-429.

Griggs, R., et al. (2015). "High resolution infrared spectroscopy: Reliable, rapid diagnosis of colorectal cancer in the colon." International Journal of Surgery **23**: S53.

Haggar, F. A. and R. P. Boushey (2009). "Colorectal cancer epidemiology: incidence, mortality, survival, and risk factors." Clinics in colon and rectal surgery **22**(04): 191-197.

Hossain, Z., et al. (2008). "Growth inhibition and induction of apoptosis of colon cancer cell lines by applying marine phospholipid." Nutrition and cancer **61**(1): 123-130.

Jackson, M., et al. (1998). "Infrared microscopic functional group mapping and spectral clustering analysis of hypercholesterolemic rabbit liver." Cellular and molecular biology (Noisy-le-Grand, France) **44**(1): 89-98.

Kazarian, S. and K. Chan (2006). "Applications of ATR-FTIR spectroscopic imaging to biomedical samples." Biochimica et Biophysica Acta (BBA)-Biomembranes **1758**(7): 858-867.

Kendall, C., et al. (2009). "Vibrational spectroscopy: a clinical tool for cancer diagnostics." Analyst **134**(6): 1029-1045.

KINDER, C. Z. and R. JM WESSELS (1997). "Gamma-irradiation and UV-C light-induced lipid peroxidation: a Fourier transform-infrared absorption spectroscopic study." International journal of radiation biology **71**(5): 561-571.

Kobayashi, D., et al. (1998). "Suppression of intracellular resistance factors by adriamycin augments heat-induced apoptosis via interleukin-1 β -converting enzyme activation in pancreatic carcinoma cells." International journal of cancer **76**(4): 552-555.

Krishnakumar, N., et al. (2009). "Chemopreventive efficacy of piperine in 7, 12-dimethyl benz [a] anthracene (DMBA)-induced hamster buccal pouch carcinogenesis: an FT-IR study." Food and chemical toxicology **47**(11): 2813-2820.

Kune, G. A., et al. (1988). "Colorectal cancer risk, chronic illnesses, operations, and medications: case control results from the Melbourne Colorectal Cancer Study." Cancer research **48**(15): 4399-4404.

Leskovjan, A. C., et al. (2010). "Fourier transform infrared imaging showing reduced unsaturated lipid content in the hippocampus of a mouse model of Alzheimer's disease." Analytical chemistry **82**(7): 2711-2716.

Lewis, P. D., et al. (2010). "Evaluation of FTIR spectroscopy as a diagnostic tool for lung cancer using sputum." BMC cancer **10**(1): 640.

Li, J., et al. (2005). "Oncogenic K-ras stimulates Wnt signaling in colon cancer through inhibition of GSK-3 β ." Gastroenterology **128**(7): 1907-1918.

Li, L., et al. (2015). "Histone deacetylase inhibitor sodium butyrate suppresses DNA double strand break repair induced by etoposide more effectively in MCF-7 cells than in HEK293 cells." BMC biochemistry **16**(1): 2.

Marks, P. A., et al. (2004). "Histone deacetylase inhibitors." Advances in CANCER RESEARCH **91**: 137-168.

Minucci, S. and P. G. Pelicci (2006). "Histone deacetylase inhibitors and the promise of epigenetic (and more) treatments for cancer." Nature reviews. Cancer **6**(1): 38.

Morisaki, N., et al. (1982). "Fatty acid specificity in the inhibition of cell proliferation and its relationship to lipid peroxidation and prostaglandin biosynthesis." Lipids **17**(12): 893-899.

Mourant, J., et al. (2003). "FTIR spectroscopy demonstrates biochemical differences in mammalian cell cultures at different growth stages." Biophysical journal **85**(3): 1938-1947.

Mourant, J., et al. (2003). "FTIR spectroscopy demonstrates biochemical differences in mammalian cell cultures at different growth stages." Biophysical journal **85**(3): 1938-1947.

Ozek, N. S., et al. (2014). "Structural and functional characterization of simvastatin-induced myotoxicity in different skeletal muscles." Biochimica et Biophysica Acta (BBA)-General Subjects **1840**(1): 406-415.

ÖZEK, N. Ş. (2015). CHARACTERIZATION OF MOLECULAR-LEVEL CHANGES DUE TO MICRORNA-125B EXPRESSION IN BREAST CANCER CELLS BY SPECTROSCOPIC AND CHEMOMETRIC ANALYSIS TECHNIQUES, MIDDLE EAST TECHNICAL UNIVERSITY.

Rada-Iglesias, A., et al. (2007). "Butyrate mediates decrease of histone acetylation centered on transcription start sites and down-regulation of associated genes." Genome research **17**(6): 708-719.

Ramesh, J., et al. (2002). "Spectroscopic evidence for site-specific cellular activity in the tubular gland in human intestine." European Biophysics Journal **30**(8): 612-616.

Rashidi, A. and A. F. Cashen (2015). "Belinostat for the treatment of relapsed or refractory peripheral T-cell lymphoma." Future Oncology **11**(11): 1659-1664.

Rigas, B., et al. (1990). "Human colorectal cancers display abnormal Fourier-transform infrared spectra." Proceedings of the National Academy of Sciences **87**(20): 8140-8144.

Ropero, S. and M. Esteller (2007). "The role of histone deacetylases (HDACs) in human cancer." Molecular oncology **1**(1): 19-25.

Saharan, R., et al. (2011). "HDAC inhibitors: a new armour in anti-cancer therapeutics." Pharmacophore **2**: 104-113.

Saharan, R., et al. (2011). "HDAC inhibitors: a new armour in anti-cancer therapeutics." Pharmacophore **2**: 104-113.

Salman, A., et al. (2001). "FTIR microscopic characterization of normal and malignant human colonic tissues." Cell Mol Biol (Noisy-le-grand) **47**: 159-166.

Severcan, F., et al. (2010). "FT-IR spectroscopy in diagnosis of diabetes in rat animal model." Journal of biophotonics **3**(8-9): 621-631.

Severcan, F., et al. (2005). "Rapid monitoring of diabetes-induced lipid peroxidation by Fourier transform infrared spectroscopy: evidence from rat liver microsomal membranes." Analytical biochemistry **339**(1): 36-40.

Severcan, F. and P. I. Haris (2012). Vibrational spectroscopy in diagnosis and screening, IOS Press.

Shadan, F., et al. (1994). "n-Butyrate, a cell cycle blocker, inhibits the replication of polyomaviruses and papillomaviruses but not that of adenoviruses and herpesviruses." Journal of Virology **68**(8): 4785-4796.

Soldatenkov, V. A., et al. (1998). "Sodium butyrate induces apoptosis and accumulation of ubiquitinated proteins in human breast carcinoma cells." Cell Death & Differentiation **5**(4).

Turker, S., et al. (2014). "Investigation of compositional, structural, and dynamical changes of pentylenetetrazol-induced seizures on a rat brain by FT-IR spectroscopy." Analytical chemistry **86**(3): 1395-1403.

Weichert, W., et al. (2008). "Expression of class I histone deacetylases indicates poor prognosis in endometrioid subtypes of ovarian and endometrial carcinomas." Neoplasia **10**(9): 1021-1027.

Zendehdel, R., Masoudi-Nejad, A., Mohammadzadeh, J., & Shirazi, F. H. (2012). Cisplatin resistant patterns in ovarian cell line using FTIR and principle component analysis. Iranian journal of pharmaceutical research: IJPR, 11(1), 235.

Zeng, H., Lazarova, D. L., & Bordonaro, M. (2014). Mechanisms linking dietary fiber, gut microbiota and colon cancer prevention. World journal of gastrointestinal oncology, 6(2), 41.

